TECHNICAL MEMORANDUM

737

Arctic sea ice in the ECMWF MyOcean2 ocean reanalysis ORAP5

S. Tietsche, M. A. Balmaseda, H. Zuo, K. Mogensen

Research Department

October 2014

European Centre for Medium-Range Weather Forecasts
Europäisches Zentrum für mittelfristige Wettervorhersage
Centre européen pour les prévisions météorologiques à moyen terme

Series: ECMWF Technical Memoranda

A full list of ECMWF Publications can be found on our web site under:
http://www.ecmwf.int/publications/

Contact: library@ecmwf.int

European Centre for Medium-Range Weather Forecasts
Shinfield Park, Reading, RG2 9AX, England

Contents

List of Figures

List of Tables

Abstract

We discuss the state of Arctic sea ice in ORAP5, a prototype for the ORAS5 ocean reanalysis, that was run as the ECMWF contribution to MyOcean2. It runs at a high spatial resolution of $1/4$ degrees. Among other innovations, ORAP5 for the first time assimilates observations of sea ice concentration. We focus on the more recent period 1993–2012, and on evaluating model performance with respect to recent observations of sea ice thickness.

We find that sea ice concentration fields in ORAP5 are very close to observations in general, with root mean square analysis residuals of less than 5% in most regions. However, larger differences in sea ice concentration between ORAP5 and observations exist for the Labrador Sea and east of Greenland during winter. In coastal areas, the model consistently simulates lower sea ice concentration than observed, which is probably due to problems with sea ice concentration observations in conjunction with the high model resolution.

Sea ice thickness is evaluated against three different observational data sets that have sufficient spatial and temporal coverage: ICESat, IceBridge and SMOSIce. Large-scale features like the gradient between the thickest ice in the Canadian Arctic and thinner ice in the Siberian Arctic are simulated by ORAP5. However, some biases remain. Of special note is the model's tendency to accumulate too thick ice in the Beaufort Gyre. The root mean square error of ORAP5 sea ice thickness with respect to ICESat is 1.0m, which is on par with the well-established PIOMAS sea ice reconstruction. Interannual variability and trend of sea ice volume in ORAP5 also compare well with PIOMAS and ICESat estimates.

Validation of thin sea ice areas against SMOSIce is a promising prospect for future operational developments, but initial analysis shows that improvements in both observations and model are necessary before this can be done consistently.

We conclude that the overall state of Arctic sea ice in ORAP5 is in reasonable agreement with observations and will provide useful initial conditions for seasonal predictions. Nevertheless, the simulation of sea ice thickness remains to be a challenge.

1 Introduction

Sea ice is a key component of polar weather and climate. Therefore, realistic estimates of sea ice initial conditions are essential for sub-seasonal, seasonal, and even interannual climate predictions in the Arctic and possibly beyond (e.g. Balmaseda *et al.* (2010); Tietsche *et al.* (2013b); Msadek *et al.* (2014)). At ECMWF, in the near future these sea ice initial conditions will be provided by an assimilation system building on the ocean reanalysis ORAP5. Therefore, we evaluate in this memorandum the state of Arctic sea ice in ORAP5 for the period 1993–2012.

ORAP5 (Ocean ReAnalysis Pilot 5) is a global ocean reanalysis produced by the ECMWF as a contribution to the EU MyOcean2 project. ORAP5 covers the period from 01 January 1979 to 31 December 2012, and it has been produced using version 3.4 of the NEMO ocean model (Madec, 2008) at a resolution of 1/4 of degree in the horizontal and 75 levels in the vertical, with variable spacing (the top level has 1m thickness). It also includes the dynamic-thermodynamic sea-ice model LIM2 (Fichefet and Maqueda, 1997). The reanalysis is conducted with NEMOVAR in a 3D-var configuration (Mogensen *et al.*, 2012). NEMOVAR is used to assimilate subsurface temperature, salinity, sea-ice concentration and sea-level anomalies, using a 5 day assimilation window. The observation information is also used via an adaptive bias correction scheme (Balmaseda *et al.*, 2013). In addition, gridded SST daily analyses are used to correct the surface heat fluxes, and information on global-average sea level trends act as constraint for the global fresh-water budget. ORAP5 surface forcing comes from ERA-Interim (Dee *et al.*, 2011), and

includes the impact of surface waves in the exchange of momentum and turbulent kinetic energy (Janssen *et al.*, 2013).

The remainder of this technical memorandum is organised as follows: after describing the methods used to produce the ocean reanalysis in Section 2, we briefly evaluate the state of sea ice concentration (SIC) in the Arctic in Section 3. The evaluation of sea ice thickness (SIT) in Section 4 is much more elaborate, because SIT is (i) arguably more important as an initial condition for predictions on sub-seasonal and longer time scales and (ii) poorly constrained by observations. Looking forward, we make some comments and suggestion for future development of the methods in Section 5, before summarising our findings in Section 6.

2 The ORAP5 setup

The NEMO ocean model version 3.4 has been used for ORAP5 in the DRAKKAR ORCA025.L75 global conguration. This conguration has a global tripolar grid with a resolution of 1/4 degree at the equator. One of the poles is located on the Antarctic continent, and the other two are in Central Asia and North Canada. Horizontal resolution in northern hemisphere high latitudes ranges from less than 5 km (Canadian Archipelago south of Victoria Island) to about 17 km (Bering Sea and Sea of Okhotsk). There are 75 vertical levels, with level spacing increasing from from 1 m at the surface to 200 m in the deep ocean. For further details on the ocean model see Madec (2008) and Zuo *et al.* (2014).

The sea ice model used for ORAP5 is LIM2 (Fichefet and Maqueda, 1997), which is run with a viscous-plastic rheology and coupled to the ocean model every three time steps. LIM2 has a simple two-category approach to model the subgrid-scale ice thickness distribution, and calculates vertical heat flux within the ice according to the three-layer Semtner scheme (Semtner, 1976). Snow on sea ice is modelled, but melt ponds are not.

Forcing fields for the ORAP5 ocean reanalysis are derived from the ECMWF atmospheric reanalysis ERA-Interim (Dee *et al.*, 2011). Observations of ocean temperature and salinity, sea level anomalies, and sea ice concentration are assimilated into NEMO/LIM2 by the NEMOVAR assimilation system (Mogensen *et al.*, 2012) in 3D-Var mode. A bias correction scheme (Balmaseda *et al.*, 2007) has been implemented in NEMOVAR to correct temperature/salinity biases in the extra-tropical regions, and pressure bias in the tropical regions. In situ profiles of temperature and salinity are taken from the quality-controlled EN3 dataset (Ingleby and Huddleston, 2007), and satellite along-track sea level anomalies are taken from the AVISO dataset. For further details see Zuo *et al.* (2014). Sea surface temperatures in the model are restored to observed values by imposing an additional heat flux of 200 W m^{-2} K^{-1}.

Observations of sea surface temperature and sea ice concentration are taken from different observational products over the time period 1993–2012:

- 01 Jan 1993 – 31 Dec 2007: UK Met Office Operational Sea Surface Temperature And Sea Ice Analysis (OSTIA, Donlon *et al.* (2012)) – *reanalysis product*
- 01 Jan 2008 – 31 Dec 2008: NOAA Optimal Interpolation 1/4 degree daily SST analysis (OIv2d2, Reynolds *et al.* (2007))
- 01 Jan 2009 – 31 Dec 2012: *operational* OSTIA product (Donlon *et al.*, 2012).

Daily gridded sea ice concentration which is provided together with sea surface temperature is assimilated. The assimilation of sea ice concentration is univariate. Standard deviations for sea ice concentration errors are assumed to be constant for simplicity: 20% for the observation error, 5% for the

Simulation	*Description*
CTRL	Control simulation with ORCA025, forced with ERA-Interim
ORAP5	Ocean reanalysis with ORCA025, forced with ERA-Interim and assimilating ocean observations as described in Section 2.
ORAP5-LR	As ORAP5, but using a lower resolution in the ocean model (ORCA1), and with a 10-day instead of 5-day assimilation window.
PIOMAS	The PIOMAS sea ice reconstruction by Schweiger *et al.* (2011).
NUDGE	A simulation with ORCA1 forced by ERA-Interim and sea ice concentration nudged towards observations (Tang *et al.*, 2013).

Table 1: Overview of model simulations and their short identifiers used throughout the text.

background error. The horizontal de-correlation length scale for background errors of sea ice concentration is 50 km, but is reduced to about 25km at the coast. Sea ice observations are thinned by a factor of 2 to reduce the data density and to speed up convergence in the cost function.

To judge the quality of ORAP5, comparison to previous model simulations is very helpful. In Table 1 we present the model simulations and their acronyms we use throughout the text. Except for PIOMAS, they have all been carried out at ECMWF.

3 Evaluation of sea ice concentration and extent

In this section, we discuss the simulation of sea ice concentration and extent in ORAP5 as compared with

- OSTIA-derived SIC (see Section 2),
- Climate data record SIC produced by the Goddard Space Flight Centre by combining retrievals from the NASA team and the Bootstrap algorithms (Peng *et al.* (2013), data available at `http://nsidc.org/data/g02202`)
- the sea ice index provided by NSIDC (Fetterer *et al.*, 2002),
- and the CTRL model simulation (see Table 1).

In general, there is very good large-scale agreement between sea ice concentration fields in OSTIA and ORAP5. As an example, Figure 1 shows sea ice concentration fields for March, July and September 2012. There are hardly any visible differences between OSTIA and ORAP5. Comparing to GSFC as an independent observational data set, it can be seen that the ice edge is almost perfectly constrained for these three example months. In the interior of the ice pack, however, GSFC has higher ice concentration than OSTIA and ORAP5 in July. This relates to well-known uncertainties of observing sea ice concentration in the melt season, when ice and snow are wet and melt ponds are present (Comiso and Kwok, 1996).

As an overall performance measure, we calculate the root mean square differences between OSTIA and ORAP5 for each month of the year from 1993 to 2012. The results for the months of March and September are shown in Fig. 2. Note that the dominance of white colours means that SIC RMSE is mostly below 5 %. However, two features with higher SIC RMSE are apparent: (i) In winter, the Labrador Sea and the east coast of Greenland exhibit errors of up to 20%, and (ii) coastal grid cells exhibit higher RMSE.

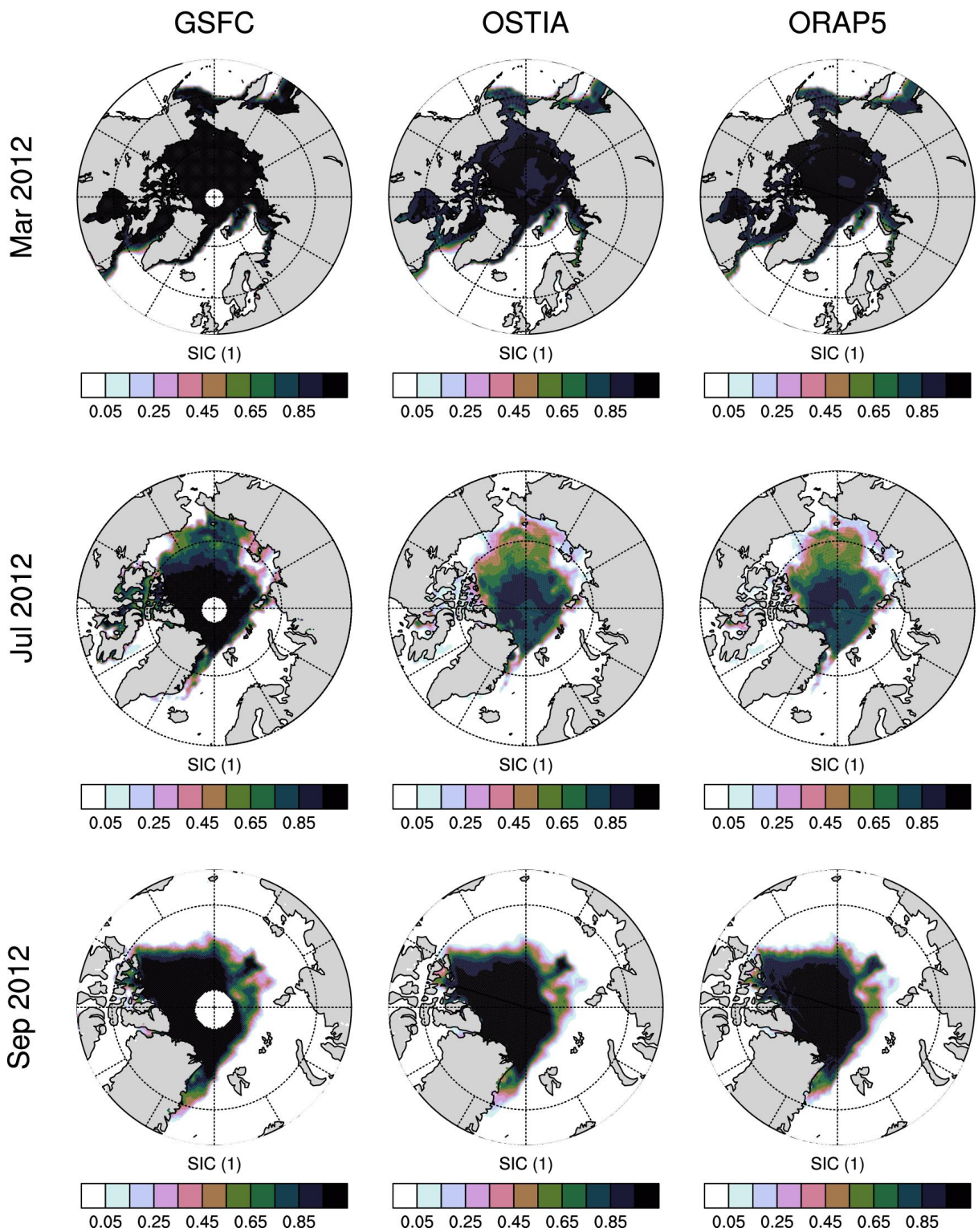

Figure 1: Sea ice concentration for March 2012 (upper row), July 2012 (middle row) and September 2012 (bottom row). The left column shows observations produced by the GSFC (Peng et al., 2013), the middle column OSTIA-derived observations. The right column is the ORAP5 reanalysed sea ice concentration.

The first problem is most likely due to errors in water mass properties, although no detailed investigation is carried out here. We only note that the RMSE shown in Figure 2 are associated with a complex bias pattern (not shown), so that a single cause for the high RMSE seems unlikely. In ORAP5, sea ice extends too far off the coast of Greenland between Spitsbergen and Iceland, whereas there is too little sea ice in the East Greenland Current south of Iceland. The western part of the Labrador Sea has too little sea ice, whereas the eastern part has too much.

We suspect that the second problem, an increased RMSE in coastal areas, is related to problems in the SIC observations. SIC observations close to the coast, where the footprint of the satellite passive microwave instrument contains land surface, are potentially unreliable. As discussed for example by Cavalieri *et al.* (1999) and Buehner *et al.* (2014), careful corrections are necessary to minimize the land-to-ocean spillover effect, which often leads to spuriously high sea ice concentrations close to the coast. This becomes more problematic with higher model resolution; for ORAP5, the footprints of the passive microwave instruments are generally larger than the model grid cells.

We show in Fig. 3 the average difference between OSTIA and ORAP5 SIC for July, the month were the effect is strongest. Note that coast lines are not drawn on the map, but can easily be traced from the increased SIC difference. An example of evident observational error in OSTIA is the Baltic Sea, which in OSTIA has extensive sea ice cover in July, in stark contrast to the ground truth provided by thousands of holiday goers. Inspection of individual years (not shown) reveals that the problem disappeared with the switch from the OSTIA reanalysis to the OSTIA operational product. Most likely, in the OSTIA operational product the additional empirical cross-check with 2m air temperature removes the excess ice along the coastlines.

So far, we have only considered the time-averaged errors and biases. However, when using the simulated sea ice state as an initial condition for seasonal predictions, it is equally important to have a good representation of the temporal evolution of deviations from the mean state. To keep the discussion concise and allow easy interpretation, we restrict ourselves to time series of the Northern Hemisphere sea ice extent (SIE), which is defined as the area of the ocean with a sea ice concentration above 15%. This widely used climate index captures large scale year-to-year fluctuations of the sea ice state as well as the strong decreasing trend in sea ice cover over the last 20 years.

Figure 4 shows SIE for ORAP5 compared to SIE for OSTIA observations, the NSIDC sea ice index (Fetterer *et al.*, 2002), and SIE for the CTRL model simulation. In general, both trend and year-to-year fluctuations of SIE agree reasonably well between ORAP5 and both observational data sets. However, the problematic high sea ice concentration in the observations discussed in the previous paragraphs (cp. Figure 3) causes SIE in OSTIA to be between 0.5 and $2 \cdot 10^6$ km higher than in ORAP5. There is a strong seasonal dependence of the bias, but it stays fairly constant from 1993 to 2008 for any given month. Interestingly, most of the time SIE in the ORAP5 reanalysis agrees better with the independent NSIDC SIE than with the OSTIA SIE, the observational product which is assimilated.

A striking feature in Figure 4 is the convergence of the different SIE curves after 2008. This is interesting given that in 2008 there is a change in the sea ice concentration observations going into the assimilation system of ORAP5 (see Section 2). To get a clearer picture of that, we plot in Figure 5 the monthly differences in SIE between NSIDC – OSTIA, OSTIA –ORAP5, and NSIDC – ORAP5. It can clearly be seen that until 2008, OSTIA SIE is consistently higher than NSIDC by about $1 \cdot 10^6$ km. From 2009 on, this bias disappears. The high SIE in OSTIA is not picked up by ORAP5. Given our judgement that OSTIA often has spuriously high sea ice concentration, this should be be interpreted as a success rather than a failure of the data assimilation.

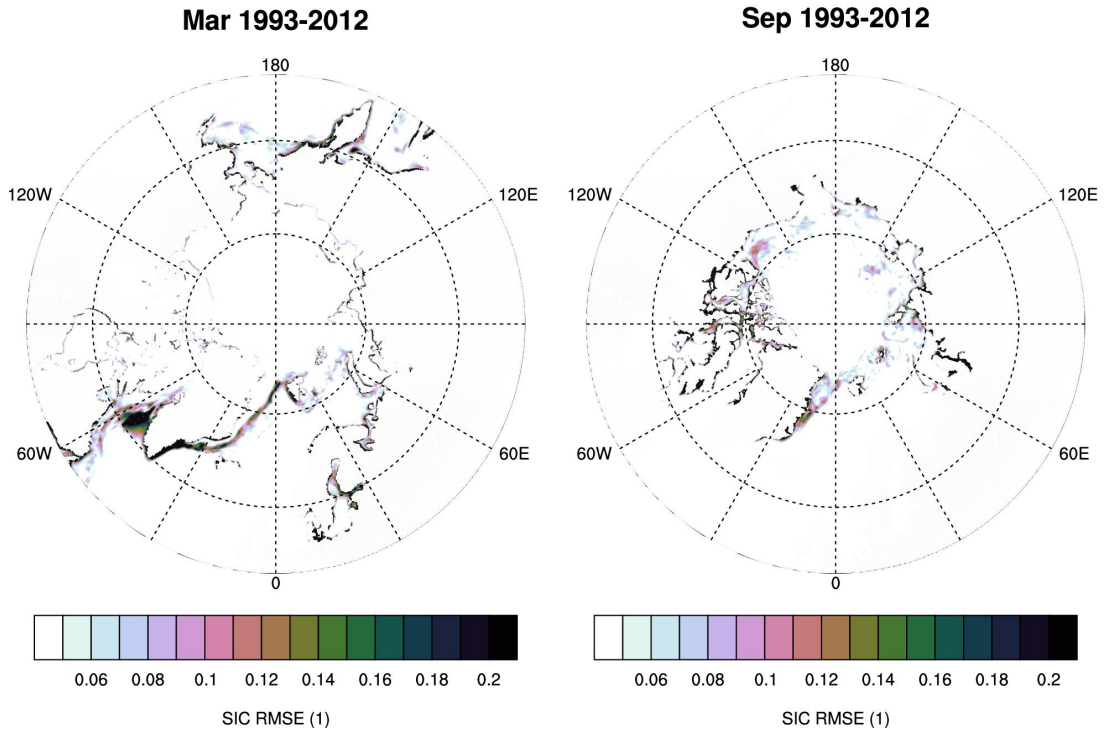

Figure 2: Root mean square analysis residuals of sea ice concentration for March (left) and September (right), averaged over 1993–2012. Coast lines are not drawn in order to make the higher analysis residuals close to the coasts visible.

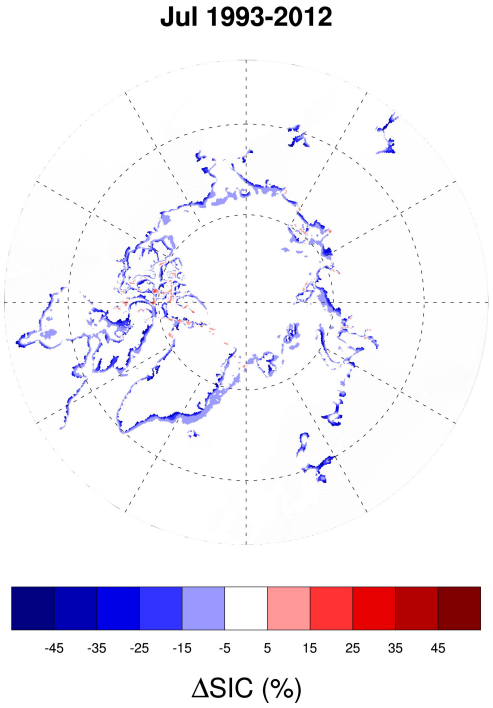

Figure 3: Analysis residuals of sea ice concentration for July, averaged from 1993–2012. It is evident that along coast lines the OSTIA-based observations are consistently higher than the analysis.

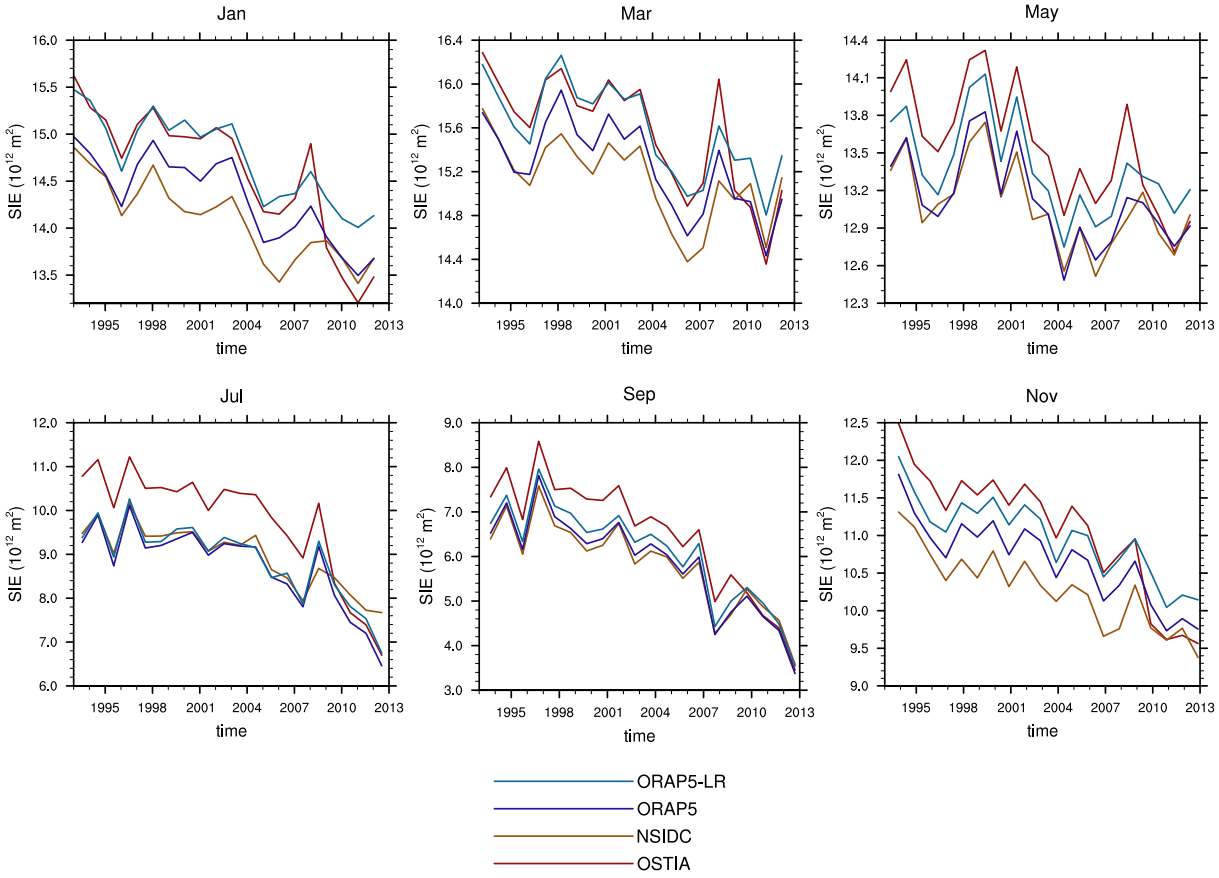

Figure 4: Sea ice extent time series from 1993 to 2012 for every other month.

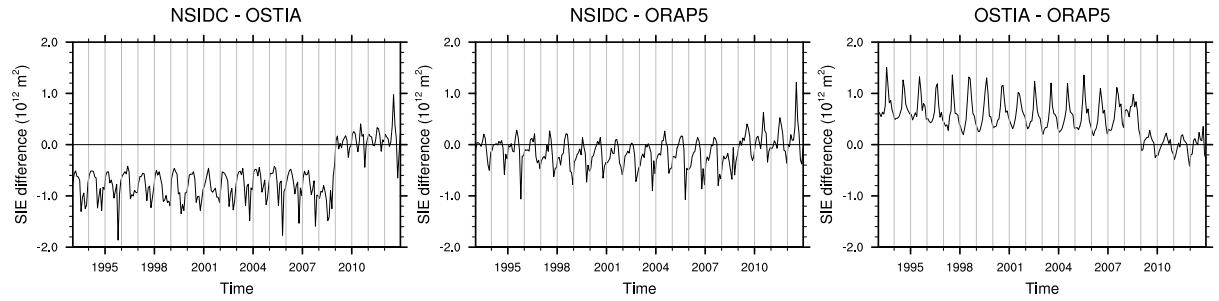

Figure 5: Difference of sea ice extent between (left) NSIDC and OSTIA observations, (middle) OSTIA and ORAP5, and (right) NSIDC and ORAP5.

Name	measurement principle	Temporal coverage	grid size
ICESat	http://nsidc.org/data/nsidc-0393		
	satellite laser altimetry	15 months from 2003 to 2008	25 km
IceBridge	http://psc.apl.washington.edu/sea_ice_cdr/data_tables.html		
	airborne laser altimetry, snow radar	Sep 2009, Mar/Apr 2010, Mar 2011, Mar/Apr 2012	50 km
SMOSIce	http://icdc.zmaw.de/l3b_smos_tb.html		
	satellite microwave brightness temperature	Oct–Mar for 2010/11/12	12.5 km
ESA-CCI	http://icdc.zmaw.de/esa-cci_sea-ice-ecv0.html		
	satellite radar altimetry	Oct–Mar 2002–2012	100 km

Table 2: Observational products for Arctic sea ice thickness with basin-scale coverage that were available at time of writing. Note that ESA-CCI sea ice thickness is still a prototype data set with uncertain quality, so that we choose not to use it for model evaluation at this time.

4 Evaluation of sea ice thickness and volume

We evaluate ORAP5 using three different sea ice thickness (SIT) observational products: laser altimeter freeboard measurements from ICESat (Kwok *et al.*, 2009), airborne laser altimeter/snow radar data from Operation IceBridge (Kurtz *et al.*, 2013), and microwave brightness temperature derived thicknesses from SMOSIce (Kaleschke *et al.*, 2012; Tian-Kunze *et al.*, 2014). Table 2 gives the relevant data sources and details of spatial and temporal coverage. We choose to evaluate ORAP5 against these three data sets because we consider them to be the most comprehensive observational data sets available at time of writing. Additionally, we compare ORAP5 to the well-established PIOMAS model reconstruction of Arctic sea ice.

4.1 What is sea ice thickness?

Before we start discussing sea ice thickness in observations and models, we would like to point out an important but easily overlooked fact: the definition of "the sea ice thickness" in a given area is not unique. Different definitions can lead to substantially different numerical values. The underlying cause for this is that the thickness of sea ice varies on very small spatial scales of a meter or even below, owing to complex small-scale sea ice processes like ridging and lead formation. Therefore, a non-trivial distribution of different in-situ sea ice thicknesses is always present in an area the size of the footprint of most satellite observation instruments, or the size of grid cells in numerical weather and climate models (see Thorndike *et al.* (1975) for a comprehensive theoretical overview).

The two most common and conflicting definitions of "the sea ice thickness" in a given grid cell are

1. $h = h_V$, the volume of ice present in the grid cell divided by the area of the grid cell, and
2. $h = h_i$, the mean ice thickness of the ice-covered part of the grid cell.

The ice thickness provided by the observational data sets we discuss here is always meant as the mean thickness of the ice-covered part of the area ($h = h_i$), whereas sea ice thickness provided by the PIOMAS sea ice model as described in Zhang and Rothrock (2001) is the volume per area ($h = h_V$). The LIM2 sea ice model, which is used for all model simulations discussed here except for PIOMAS, again outputs the mean thickness of the ice-covered fraction of the grid cell ($h = h_i$).

LI	Start	End	LI	Start	End	LI	Start	End
1	2003-02-20	2003-03-29	3B	2005-02-17	2005-03-24	3G	2006-10-25	2006-11-27
2A	2003-09-25	2003-11-19	3C	2005-05-20	2005-06-23	3H	2007-03-12	2007-04-14
2B	2004-02-17	2004-03-21	3D	2005-10-21	2005-11-24	3I	2007-10-02	2007-11-05
2C	2004-05-18	2004-06-21	3E	2006-02-22	2006-03-27	3J	2008-02-17	2008-03-21
3A	2004-10-03	2004-11-08	3F	2006-05-24	2006-06-26	3K	2008-10-04	2008-10-19

Table 3: Dates of ICESat laser campaigns. First column is the Laser Identifier String LI, second column is the first day of the laser campaign, and the third column is the last day of the laser campaign. Due to the narrow footprint of the instrument, multiple swaths during the dates given are necessary to compile a basin-wide measurement of sea ice thickness. Here and elsewhere, data are then interpreted as the mean for the given time period.

The implications for the analysis presented here are that (i) to compare with observed sea ice thickness, PIOMAS simulated sea ice thickness has to be divided by the simulated sea ice concentration, and (ii) we cannot easily obtain estimates of pan-Arctic sea ice volume from sea ice thickness observations, because they do not come with consistent sea ice concentrations observations.

4.2 ICESat laser altimetry

These sea ice thickness data were derived from measurements made by the Ice, Cloud, and Land Elevation Satellite (ICESat) Geoscience Laser Altimeter System (GLAS) instrument (Yi and Zwally, 2010). They depend on additional auxiliary data: sea ice concentration observations from the Special Sensor Microwave/Imager (SSM/I), and climatologies of snow and drift of ice. There are 15 disparate months of sea ice thickness observations available from 20 February 2003 to 19 October 2008 (see Table 3 for dates). We consider these data to be the best observations of pan-Arctic sea ice thickness to date, because (i) they have almost complete spatial coverage of sea ice occurrence in the northern hemisphere which a smaller gap around the north pole ($> 86°$N) than other observations, (ii) although not continuous in time, temporal coverage is good enough to provide a hard test of model performance (spans 5 years, seasonal cycle sampled; see Table 3), and (iii) there has been ample research on the interpretation and quality of the ICESat data (Kwok and Cunningham, 2008). For this reason, we use ICESat SIT observations as our main validation product to rank the performance of model simulations.

We start the discussion by showing two example maps of Arctic SIT, as observed by ICESat and simulated by ORAP5 and CTRL. A complete listing of all ICESat campaigns compared with ORAP5 and CTRL is provided in the Appendix A.1. For May 2006 (Figure 6) the thickest ice is observed north of the Canadian Archipelago and Greenland, with a clear gradient to thinner ice closer to the Siberian Coast. There is a lot of spatial variability on the scale of approximately 100 km, which is probably due to ridging and lead formation processes. The simulations with NEMO/LIM2 simulate the gradient from thick ice north of the Canadian Archipelago and Greenland to the Siberian side, however they show systematic biases. ORAP5 corrects the overestimation of sea ice thickness north of the Canadian Archipelago in CTRL, but also introduces an overestimation of SIT in the Beaufort Gyre. This overestimation of sea ice thickness in the Beaufort Gyre occurs in different years, in different simulations with the NEMO/LIM2 model (ORAP5-LR and NUDGE, see Table 1), and reportedly also in other ocean and climate models. Therefore, further research is warranted as to the reason for this bias. It is also worth noting that the model simulations do not reproduce the 100 km-scale variability observed by ICESat. We can only speculate that the formulation of the sea ice dynamics (viscous-plastic rheology, ridging parameterisation) is not sufficient to create this kind of spatial variability.

While the beneficial impact of SIC assimilation on the simulated SIT is apparently small for the example

shown in Figure 6, it is large for the example shown in Figure 7. Here, a strong overestimation of SIT in the Beaufort Gyre by CTRL is corrected in ORAP5. Overall, all large-scale discrepancies between ORAP5 and ICESat for October 2007 seem to be smaller than 1m. Note, however, that high SIT discrepancy is present in isolated spots, for example in the Fram Strait and close to Franz Josef Land. These isolated spots of high sea ice thickness close to the ice edge might be an artefact of the observing system, but further investigation is needed to determine this.

To obtain objective indices for the performance of different model simulations with respect to ICESat SIT observations, we calculate the root mean square error (RMSE) and the bias of the SIT fields for each observational campaign. These summarise the characteristics of SIT errors in just two numbers, allowing for convenient comparison between several model simulations and all observation times at a glance.

Figure 8 shows SIT RMSE with respect to ICESat observations for each of the 15 observed months, and for all model simulations given in Table 1. It is evident that there is large variation in model performance between observations. For instance, for the observational campaign started 17 February 2005, all model simulations have a very similar RMSE of around 1.1m. On the other hand, for the campaign started 2 October 2007, the RMSE of simulations ranges from more than 1.3m for CTRL to 0.8m for ORAP5.

There also seem to be overall trends in how well individual model simulations perform. Whereas PIOMAS RMSE is getting slightly higher in later years, ORAP5, ORAP5-LR and NUDGE clearly have lower RMSE in 2007/2008 than in previous years. As a result, PIOMAS is the best-performing model 2003–2005, whereas ORAP5 is the best-performing model 2006–2008. If one ranks the models according to their average RMSE across observational campaigns, one arrives at the ordering ORAP5, PIOMAS, ORAP5-LR, NUDGE, CTRL from best to worst (numerical values of average RMSE are given in the legend of Figure 8).

Alongside the RMSE, the bias of each simulated SIT field with respect to ICESat observations is of interest, which is shown in Figure 8. By visual inspection (and counting the number of validation times with positive/negative bias) we see that the CTRL simulation has on average thicker sea ice than observed, in agreement with the maps shown in Figures 6 and 7, whereas PIOMAS and NUDGE tend to be biased low. ORAP5 and ORAP5-LR are roughly balanced between having positive and negative field biases. If one ranks the models according to their root mean square average bias across all validation times, one arrives at the ordering ORAP5, PIOMAS, ORAP5-LR, NUDGE, CTRL from best to worst (numerical values of root-mean-square bias are given in the legend of Figure 8). Note that this is exactly the same ordering as for the RMSE, despite the fact that, from the trivial algebraic identity $\mathrm{RMSE}^2 = \sigma^2 + \mathrm{bias}^2$, with σ^2 the variance of the field differences, we would conclude that RMSE is dominated by a large variance of the error distribution, rather than by a displaced mean.

We point out that the measures discussed in the previous paragraphs are not scale-aware and will not emphasize the large-scale problems we discussed in the previous paragraphs. Therefore, should one wish to investigate simulation performance for specific months in more detail, we recommend to refer to Appendix A.1 and rely on visual inspection of the SIT fields followed by a subjective assessment of the model simulation.

To summarise the ICESat validation, we conclude that (i) the assimilation of sea ice concentration with NEMOVAR improves SIT, although high biases remain in the Beaufort Gyre, and (ii) ORAP5 performs at least as well in simulating pan-Arctic SIT as the well-established PIOMAS sea ice reconstruction.

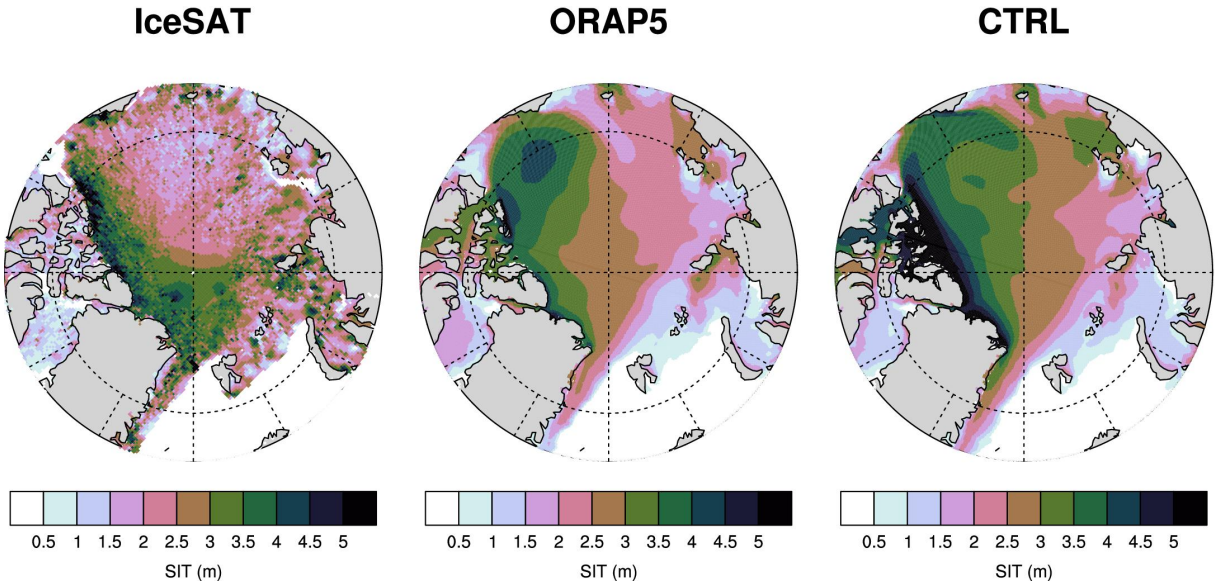

Figure 6: ICESat sea ice thickness observations (left column), model assimilation run (middle column), and model control run (right column) for May/June 2005. Note that here and elsewhere, contour data is shown on the original model or observational grid cells without any interpolation or smoothing.

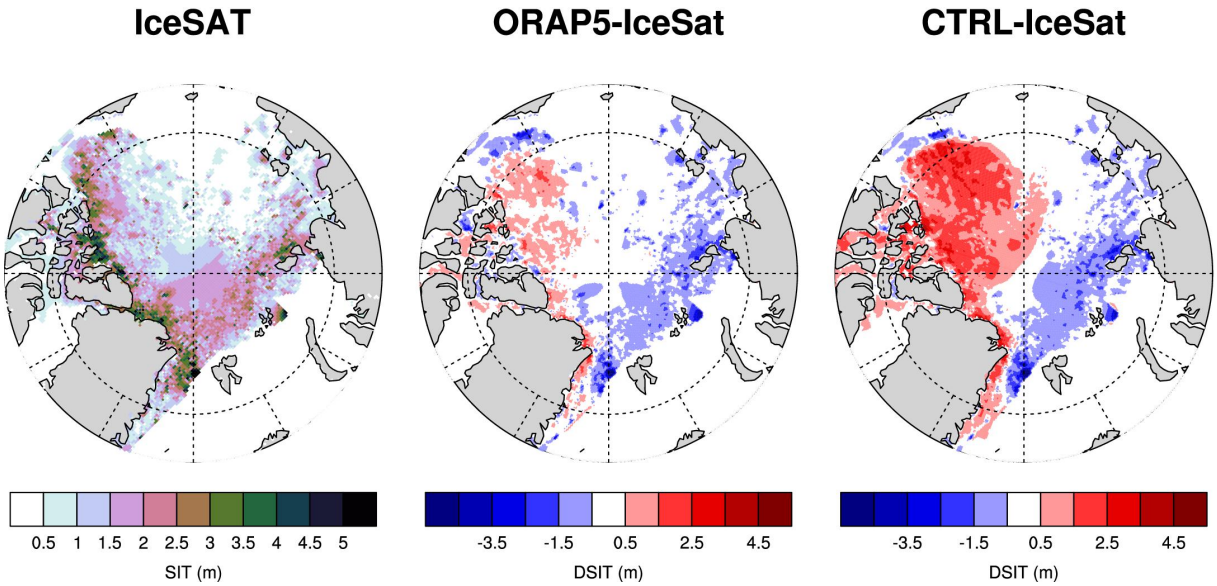

Figure 7: ICESat sea ice thickness observations (left column), difference to ORAP5 (middle column), and difference to CTRL (right column) for Oct/Nov 2007.

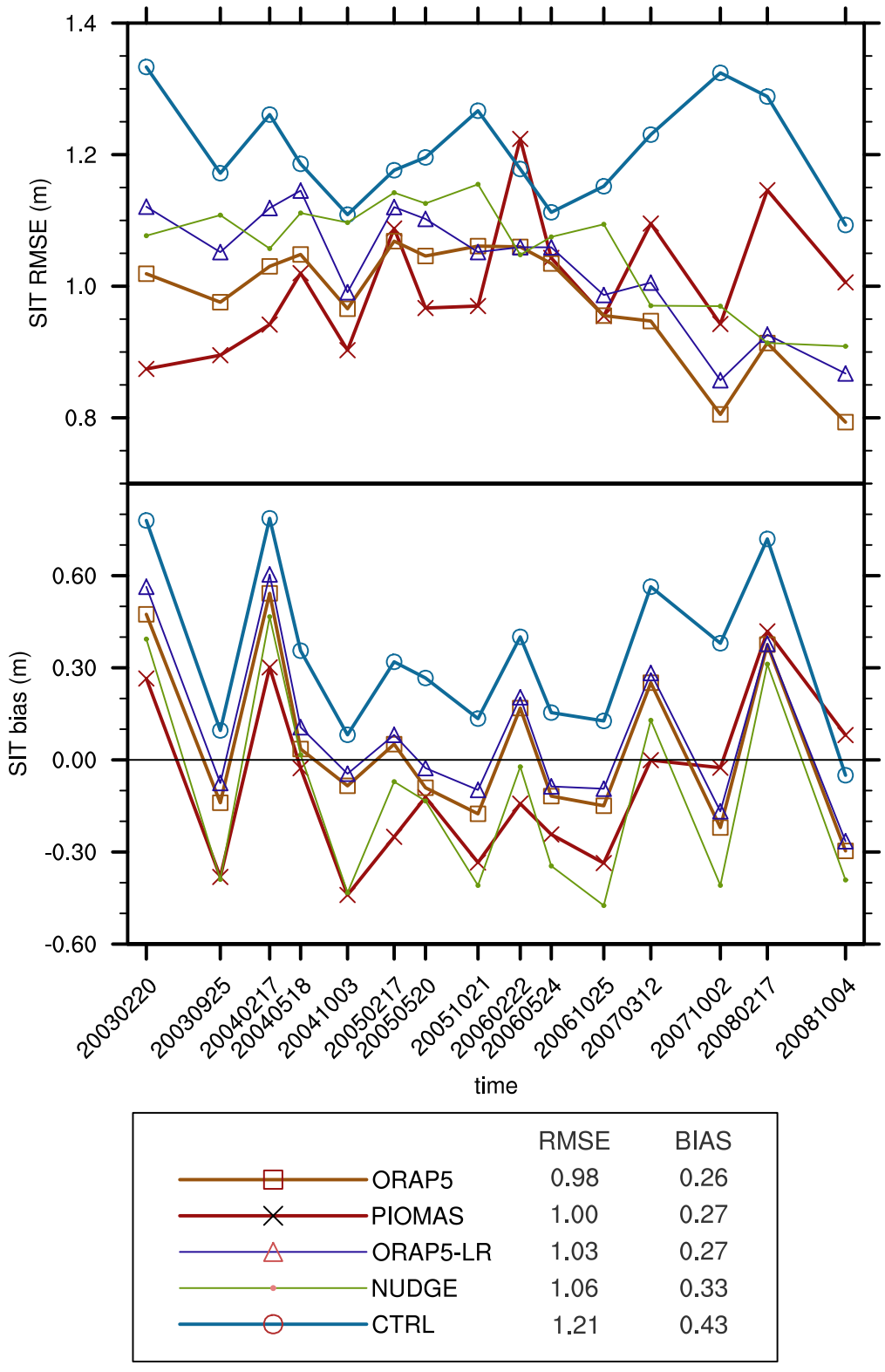

Figure 8: RMSE (top) and bias (bottom) of modelled sea-ice thickness with respect to 15 months of pan-Arctic ICESat observations. To compare the fields, ICESat data is interpolated to the model grid. Only grid cells with ICESat thickness larger than 0.5 m are considered. Time-averaged RMSE and RMS bias for each simulation are given in the legend (smaller is better).

4.3 Operation IceBridge

We use data derived from the IceBridge airborne surveys carried out each year close to the annual sea ice maximum in March/April for 2009, 2010, 2011 and 2012. These data are organised in 625 50-km clusters, each of which represents at least 500 point samples of ice thickness (Kurtz *et al.* (2013); also confer Table 2).

Figure 9 shows data from the last campaign carried out between 15 March and 11 April 2012. The data is organised in 256 50-km clusters, overlaid on the simulated ice thickness field. Figures of the remaining IceBridge observational campaign are shown in Section A.2. It can be seen that simulated SIT is not too far off observed SIT. However, substantial differences are visible, most notably a strong underestimation of sea ice thickness along the east coast of Greenland. As for ICESat observations, the observed small-scale spatial variability of SIT is not represented by the model.

The root mean square difference between IceBridge and ORAP5 computed over all 625 data points from five measurement campaigns between 2009 and 2012 is 0.97m. This is only a very slight improvement with respect to CTRL, which has an root mean square difference of 0.99m. Moreover, the bias is larger in ORAP5 (+0.39m) than in CTRL (+0.28m). There are conceptual reasons why – in the thick-ice area in the Canadian Arctic where the IceBridge data were taken – the sea ice concentration assimilation would have difficulties improving the sea ice thickness simulation (see Section 5.3). However, it is also possible that the overestimation of sea ice thickness in the IceBridge domain is related to problems with some ocean temperature and salinity observations.

We note that Figure 9 compares a monthly-mean model field with observations taken on a particular day within this month. It is desirable to construct a more refined observation operator that retrieves the model field at the same day as the observations. It is unclear at present whether this would lead to major changes in the above assessment. However, we might expect that model performance will not be much different then, because the differences between IceBridge and ORAP5 are so large (often more than 1 m) and the model SIT fields tend to vary little on the scale of days.

4.4 SMOSIce

In the SMOSIce project, the Microwave Imaging Radiometer using Aperture Synthesis (MIRAS) on board the SMOS satellite was used to derive the thickness of thin sea ice under cold conditions (Kaleschke *et al.*, 2012; Tian-Kunze *et al.*, 2014). The main advantages of the data are (i) daily coverage in polar regions, (ii) they are provided in near-real time with only 24h latency, and (iii) they have high spatial resolution (15km). The main disadvantages are (i) the limitation to thin ice of up to approximately 0.5 m, i.e. no measurements in the central Arctic, (ii) the limitation to cold surface conditions, i.e. no measurements during the melt season, and (iii) the complex error characterisation, which is still under development (Tian-Kunze *et al.*, 2014).

Despite the disadvantages of SMOSIce, the measurement of thin ice is arguably very relevant for initialising predictions. During the melt season, areas of thin sea ice will melt out quickly, changing the atmospheric boundary conditions drastically. During the cold season, thin sea ice is experiences the fastest changes because it grows quicker and is more susceptible to compression and ridging than thick sea ice (Hibler III, 1979).

Here, we compare monthly-mean model sea ice thickness with monthly mean sea ice thickness estimated from SMOS data. In Figure 10 we show examples of SMOS-derived SIT observations alongside modelled SIT from ORAP5 and CTRL during autumn 2012. It is evident that the model overestimates the

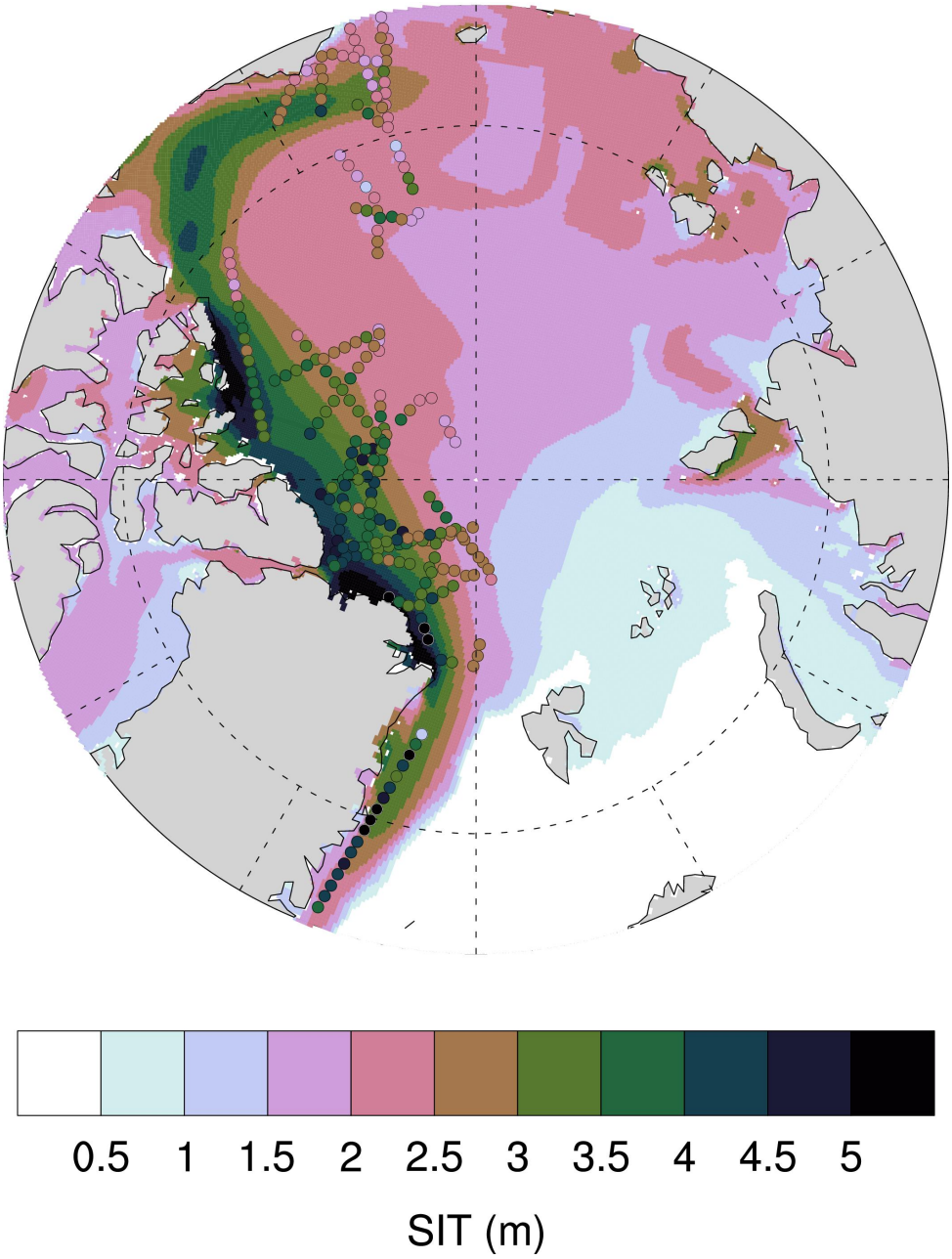

Figure 9: IceBridge ice thickness measurements from 2012/03/15 to 2012/04/11 (256 data points, coloured markers) overlayed on simulated sea ice thickness in ORAP5 for March 2012.

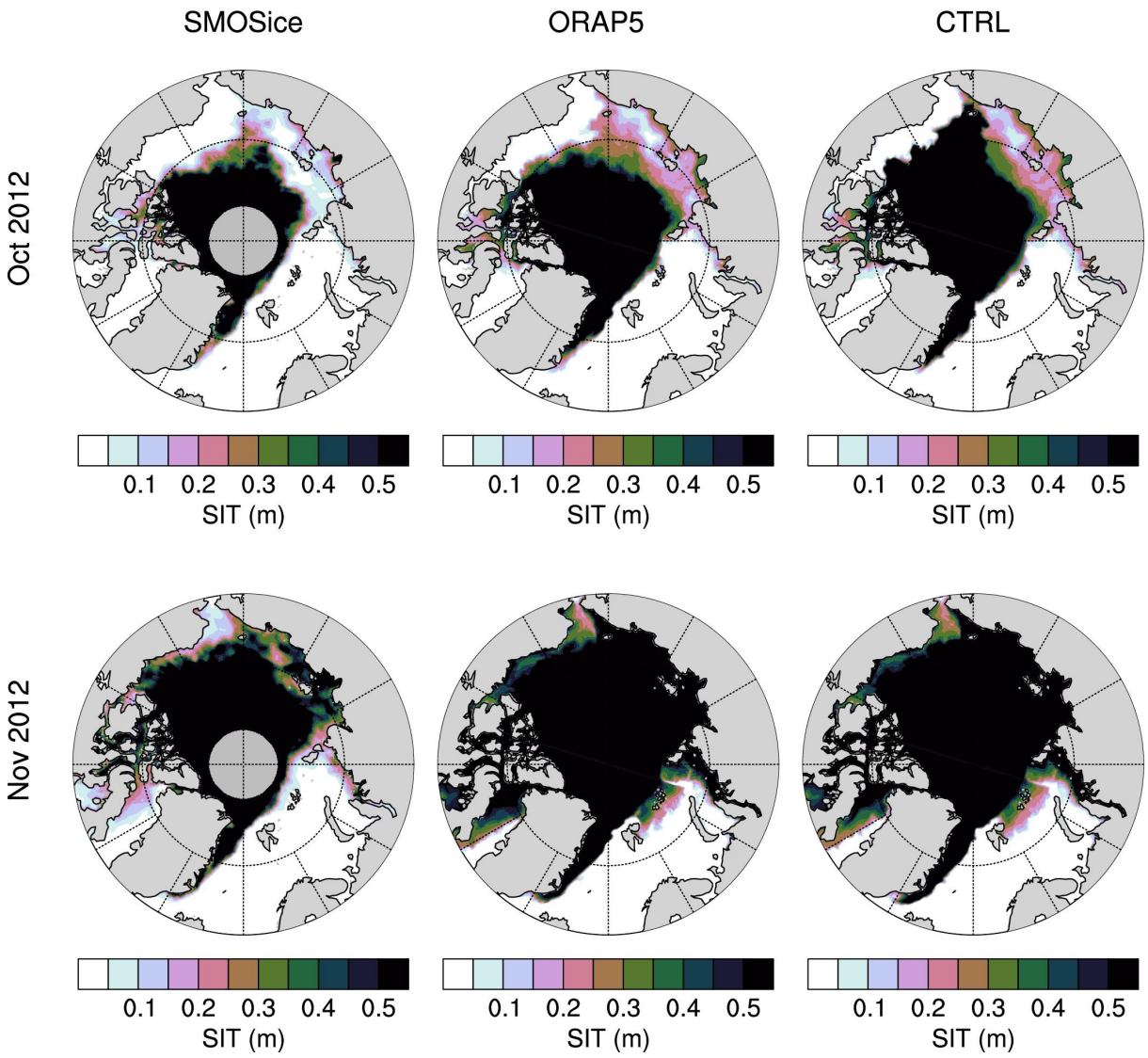

Figure 10: Sea ice thickness fields from SMOS (left), in ORAP5 (middle) and CTRL (right) for two consecutive months: October 2012 (top row) and November 2012 (bottom row). Note that the highest contour level is at 0.5 m.

thickness of thin ice in most of the marginal Seas of the Arctic Ocean where ice is newly forming from open water. There are indications that the assimilation of sea ice concentration alleviates this problem somewhat (compare reduction of SIT in East Siberian Sea and Chukchi Sea during October in ORAP5 compared to CTRL).

Note, however, that substantial underestimation of SIT are likely in the SMOSIce product when sea ice concentration is not close to 100% (Tian-Kunze *et al.*, 2014). For instance, in the Chukchi Sea in November 2012 SMOSIce diagnoses very thin ($\approx$ 10 cm) ice. In this area during the same month sea ice concentration was about 50% (GSFC) or even less (OSTIA) and SMOS brightness temperatures are around 150K. According to Figure 8 in Tian-Kunze *et al.* (2014), one should then expect SMOSIce to underestimate SIT by up to 20 cm. This would rectify the model–data mismatch in the Chukchi Sea. In other cases, like the November Barents Sea, it seems likely that the model overestimates the real sea ice thickness.

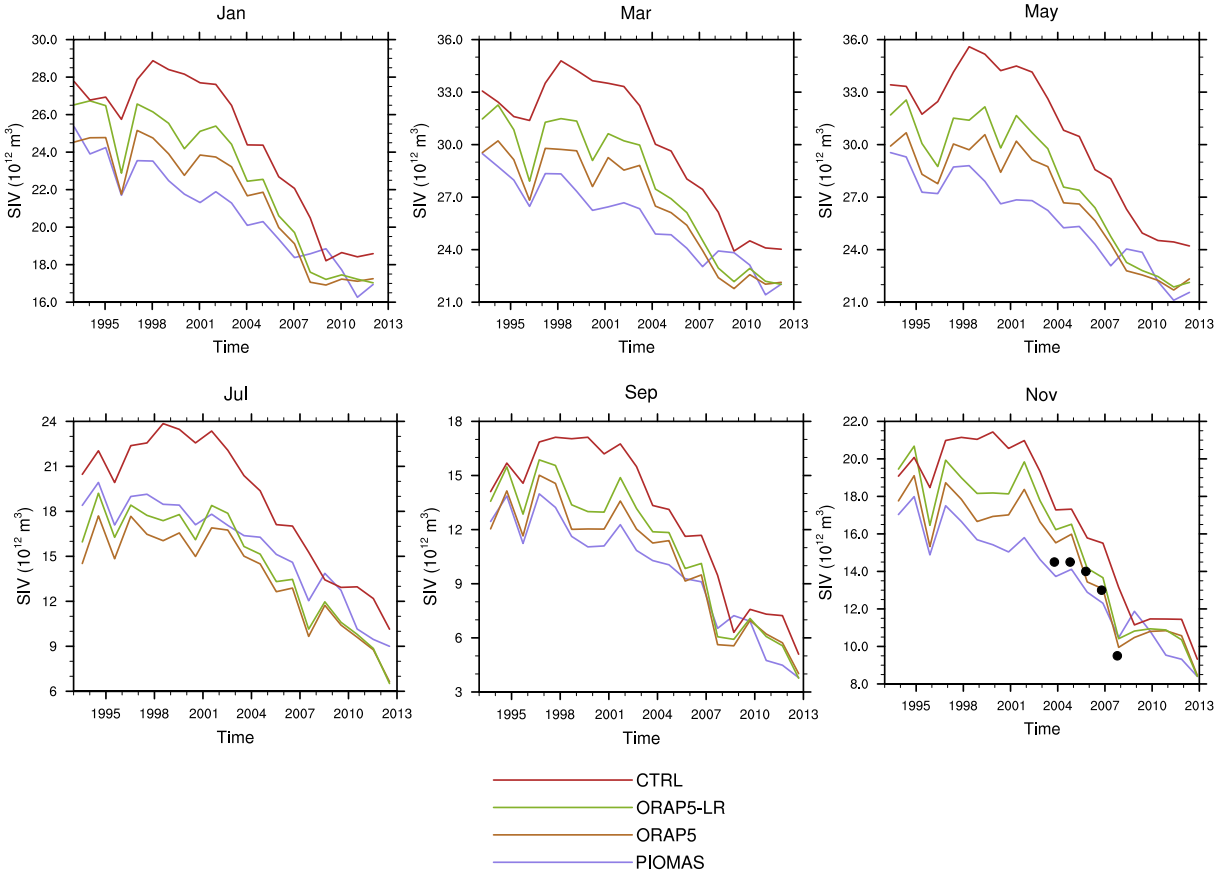

Figure 11: Sea ice volume time series from 1993 to 2012 for every other month. The black dots in the November panel are the observational volume estimates for October/November ICESat campaigns derived by Kwok et al. (2009)

4.5 PIOMAS

To evaluate whether ORAP5 simulates natural variability of the Arctic sea ice cover correctly, long observational time series over the whole Arctic are needed. For sea ice thickness, these are not available at present. Instead, we compare the ORAP5 with the well-documented and well-established PIOMAS model ice thickness reconstruction (Schweiger *et al.*, 2011). Fig. 11 shows Northern Hemisphere sea ice volume in ORAP5 and PIOMAS.

There is overall good agreement in magnitude and trend of SIV. However, a seasonally varying bias is evident: during winter months, ORAP5 has higher SIV than PIOMAS, and in July it is the other way round. There is resemblance in interannual variability, although some differences remain, especially in the last years of the simulation. Note that the simulated SIV in both runs agrees rather well with observational estimates from ICESat data (Kwok *et al.*, 2009).

5 Outlook

5.1 Limitations of the sea ice model

The formulation of the LIM2 sea ice model (Fichefet and Maqueda, 1997) used for ORAP5 simplifies the sea ice thickness distribution within a single grid cell to the maximum degree possible: a fraction C of the grid cell area is covered by thick ice of thickness h, and the remaining part of the grid cell area $1-C$ is open water. This formulation, the so-called two-category thickness approach, goes back to the late 1970s (e.g. Hibler III (1979)), and has been used in numerous numerical sea ice models.

However, it has been shown by Chevallier and Salas-Mélia (2012) that modelling the finer details of the subgridscale ice thickness distribution might be an important source of predictability for sea ice. Furthermore, the simulation of changes in sea ice concentration in the two-category approach requires unphysical assumptions: under melting conditions, one *must* assume a presupposed in-situ ice thickness distribution in the ice-covered part of the grid cell, otherwise there could be no gradual changes in ice concentration. This is conceptually inconsistent with the assumption of a constant in-situ thickness that is used to calculate conductive heat fluxes (Mellor and Kantha, 1989). Under freezing conditions, one needs to make the assumption that the ice that grows in the open-water part forms at a certain initial thickness h_0 (Hibler III, 1979). This initial thickness needs to be chosen so that the increase in sea ice concentration under freezing conditions matches observational evidence. In LIM2, the initial thickness is of the order of $h_0 = 0.5$ m. This means, however, that the first sea ice to appear in a grid cell is already 0.5 m thick yet occupies only a very small fraction of the grid cell. This is clearly not compatible with the known processes of sea ice formation observed in the real world (frazil/Nilas ice, followed by compacting pancake ice).

In summary, with the two-category thickness assumption the model is not able to adequately simulate sea ice states with $h < h_0$ on a per-timestep basis. This is a problem, because (i) thin sea ice is becoming more and more abundant in the Arctic, (ii) these thin sea ice areas are arguably very relevant for any prediction problem, and (iii) with SMOSIce there are now observational products being developed that can specifically observe these thin ice areas, but evaluation of model performance is ambiguous.

We therefore suggest that future model versions at ECMWF use multi-thickness category sea ice models like LIM3.

5.2 Robustness of results when changing model resolution

Comparison of ORAP5 with ORAP5-LR indicates that the results discussed in the previous sections are quite robust when changing the model resolution. However, it seems that Arctic sea ice is slightly better simulated in ORAP5 than in ORAP5-LR. In Figure 4, until 2008 ORAP5-LR in winter months stays in general closer to the OSTIA observations, which we consider to overestimate sea ice concentration and extent. After 2008, ORAP5-LR diverges from the sea ice extent of ORAP5 as well as the observations.

For sea ice thickness, we have seen in Figure 8 that root mean square error and bias of ORAP5-LR are comparable to, but slightly worse than, those of ORAP5. It is noteworthy that error and bias vary in the same manner between ORAP5 and ORAP5-LR, suggesting very similar sea ice thickness fields. This is corroborated by Figure 11, which shows that the temporal evolution of sea ice volume is very similar between ORAP5 and ORAP5-LR.

Despite the similarity of large-scale features between ORAP5 and ORAP5-LR, the higher resolution

of ORAP5 represents the complex coastlines and bathymetry in the Arctic much better. While this potentially allows to represent mesoscale processes and to increase fidelity of regional simulations, it also introduces new problems for the data assimilation like the coastal pollution of sea ice observations discussed by Buehner *et al.* (2014), which do not affect the lower resolution.

5.3 Improvements in sea ice data assimilation

The ocean reanalysis ORAP5 discussed here uses univariate assimilation of observed sea ice concentration C. Because the sea ice model LIM2 happens to have the in-situ sea ice thickness h_i as a prognostic variable, an assimilation increment in C with constant h_i will actually lead to a *nonzero* assimilation increment in the grid cell sea ice volume V. This might be desired, but might as well have adverse implications. For instance, Tietsche *et al.* (2013a) noted that for a given SIC assimilation increment ΔC, the implied assimilation increment of sea ice volume ΔV is proportional to the background in-situ thickness: $\Delta V = h_i \Delta C$.

As a consequence, sea ice concentration changes close to the ice edge where in-situ thickness is low will have a small impact on sea ice volume. Conversely, in areas of very thick ice like north of Greenland even a very small assimilation increment in sea ice concentration will lead to a substantial change in sea ice volume. It is highly questionable whether this appropriate for the error covariances between sea ice concentration and thickness (cp. Lisaeter *et al.* (2003)).

For future developments at ECMWF, it might be worth exploring alternative approaches of sea ice data assimilation, for instance the ad-hoc approach of having sea ice volume increments *proportional* to sea ice concentration increments, which is easy to implement and was found by Tietsche *et al.* (2013a) to give very promising results.

In the medium term, the sea ice data assimilation scheme could be substantially improved by formulating realistic flow-dependent multivariate error covariances between ice thickness, ice concentration, ice velocity, sea surface salinity and sea surface temperature. The treatment of the non-Gaussian nature of sea ice concentration and thickness errors poses an additional challenge.

6 Conclusions

Sea ice concentration in ORAP5 is well constrained by observations. There remain some regional biases (most noteworthy in wintertime Labrador Sea in the early 1990s), and coastal grid points are problematic. The remaining biases are however within the uncertainty of the observations, as a comparison between different data sets shows. The year-to-year variability of sea ice concentration and extent is well simulated.

Sea ice thickness in ORAP5 agrees at least as well with ICESat observations as PIOMAS, with a remaining pan-Arctic RMSE of 0.9 m. Comparison with a free model simulation (CTRL) shows that the simulation of ice thickness benefits from assimilation of sea ice concentration. A long-standing model bias of accumulating too thick ice in the Beaufort Gyre remains. Comparison with IceBridge data suggests that sea ice thickness north of the Canadian Archipelago and Greenland is overestimated. Preliminary comparison with SMOSIce data suggests that the model has difficulties simulating the thin ice in the vicinity of the ice edge, which might be an important aspect for future improvements of sea ice initial conditions in the seasonal prediction system. Trend and year-to-year variability of sea ice volume in ORAP5 are consistent with the PIOMAS sea ice reconstruction.

A Appendix

A.1 Additional ICESat sea ice thickness maps

Figures 12 – 16 show sea ice thickness observations for all available ICESat campaigns together with the corresponding ice thickness estimates from ORAP5 and CTRL. The figures are organised according to season:

- Figures 12 and 13: late winter and early spring (February/March/April),
- Figure 14: late spring (May/June),
- Figures 15 and 16: autumn (September/October/November).

A.2 Additional IceBridge sea ice thickness maps

Figures 17 – 20 show the sea ice thickness estimated by ORAP5 during all IceBridge observational campaigns:

- Figure 17: March/April 2009,
- Figure 18: March and early April 2010,
- Figure 19: second half of April 2010,
- Figure 20: March 2011.

The IceBridge campaign for March/April 2012, which has by far the most data points, is shown in the main text as Figure 9.

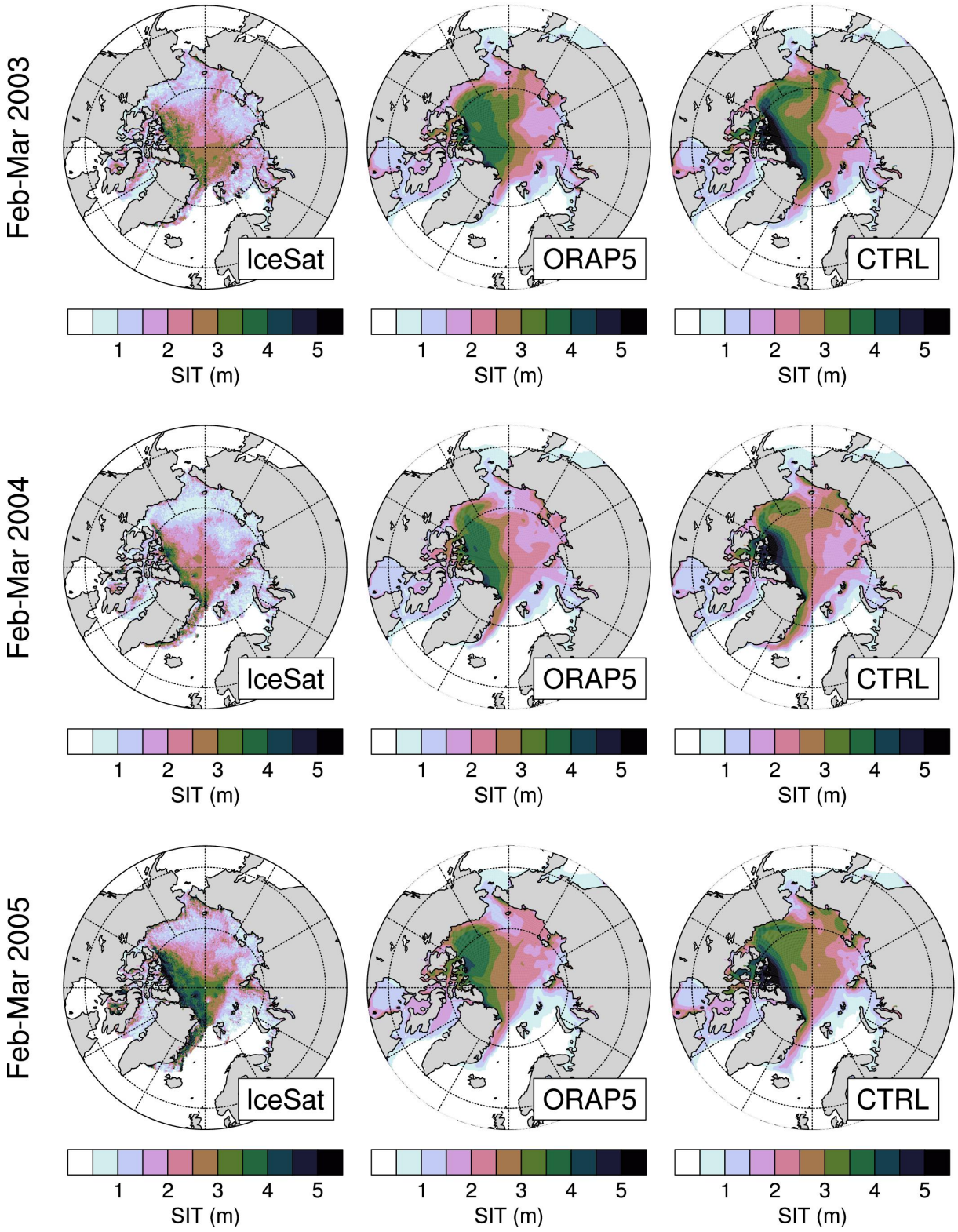

Figure 12: ICESat sea ice thickness observations (left column), ORAP5 (middle column), and CTRL (right column) for February/March/April in 2003–2005. See Table 3 for the exact dates when the observations were taken.

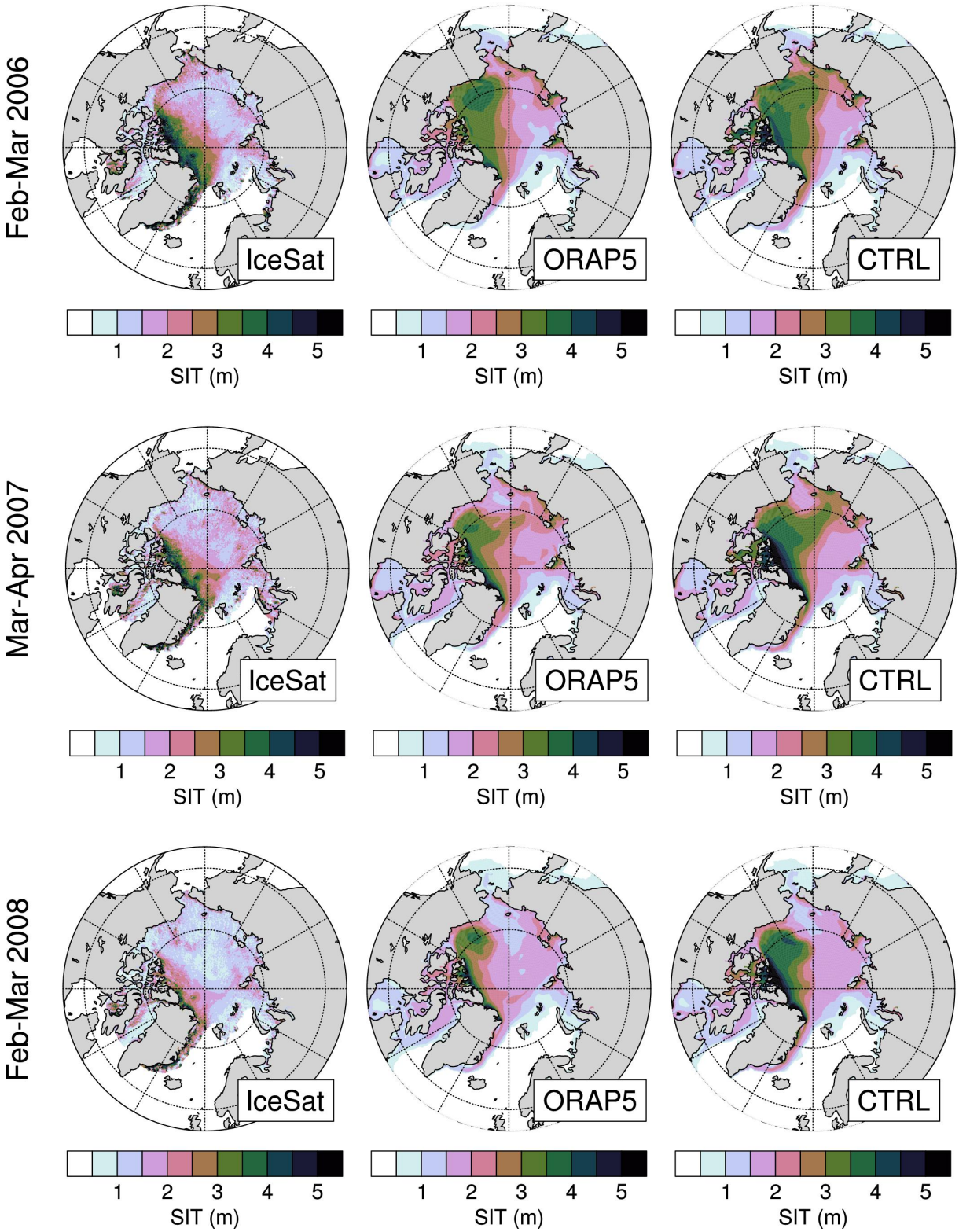

Figure 13: ICESat sea ice thickness observations (left column), ORAP5 (middle column), and CTRL (right column) for February/March/April in 2006–2008. See Table 3 for the exact dates when the observations were taken.

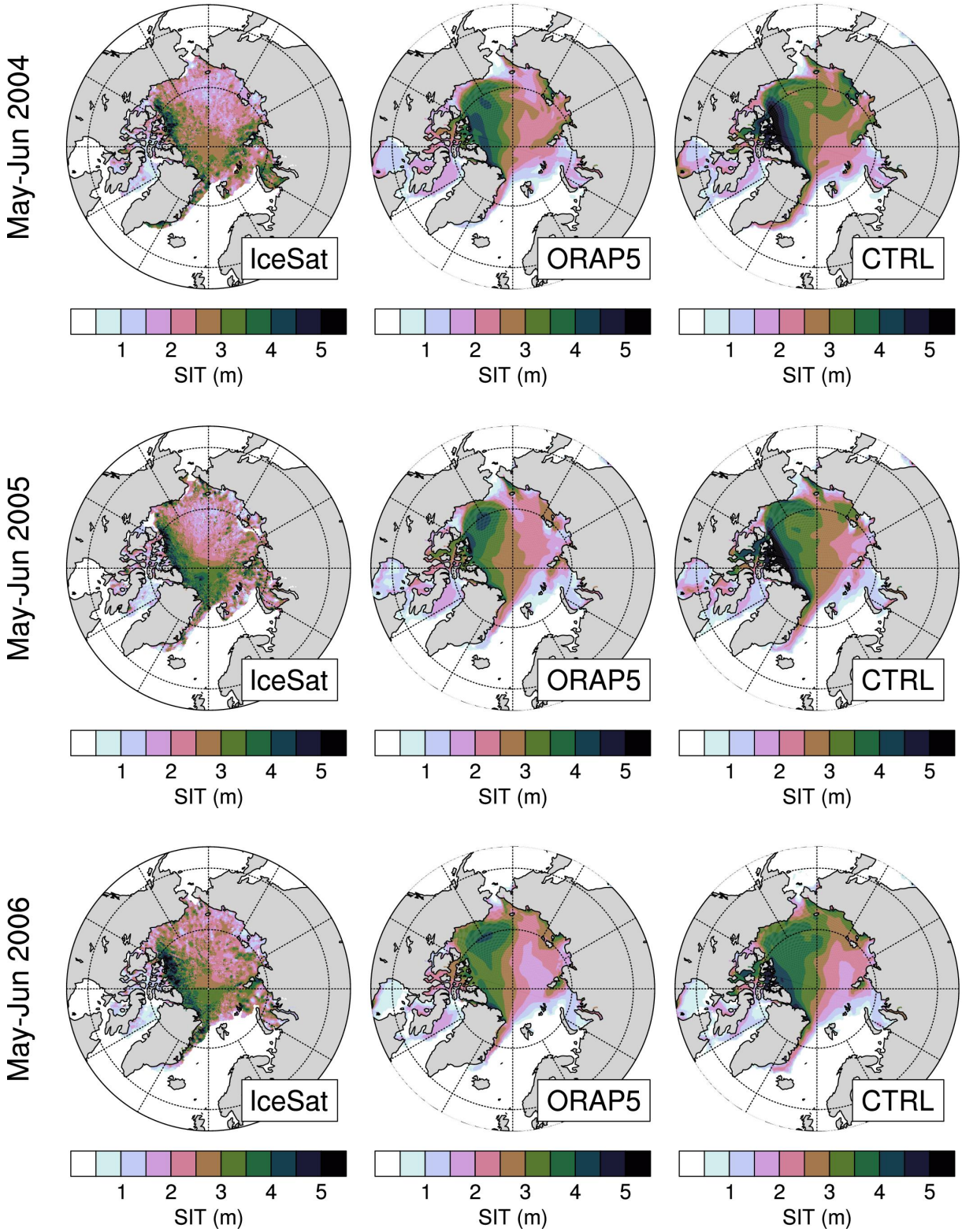

Figure 14: ICESat sea ice thickness observations (left column), ORAP5 (middle column), and CTRL (right column) for May/June in 2003–2005. See Table 3 for the exact dates when the observations were taken.

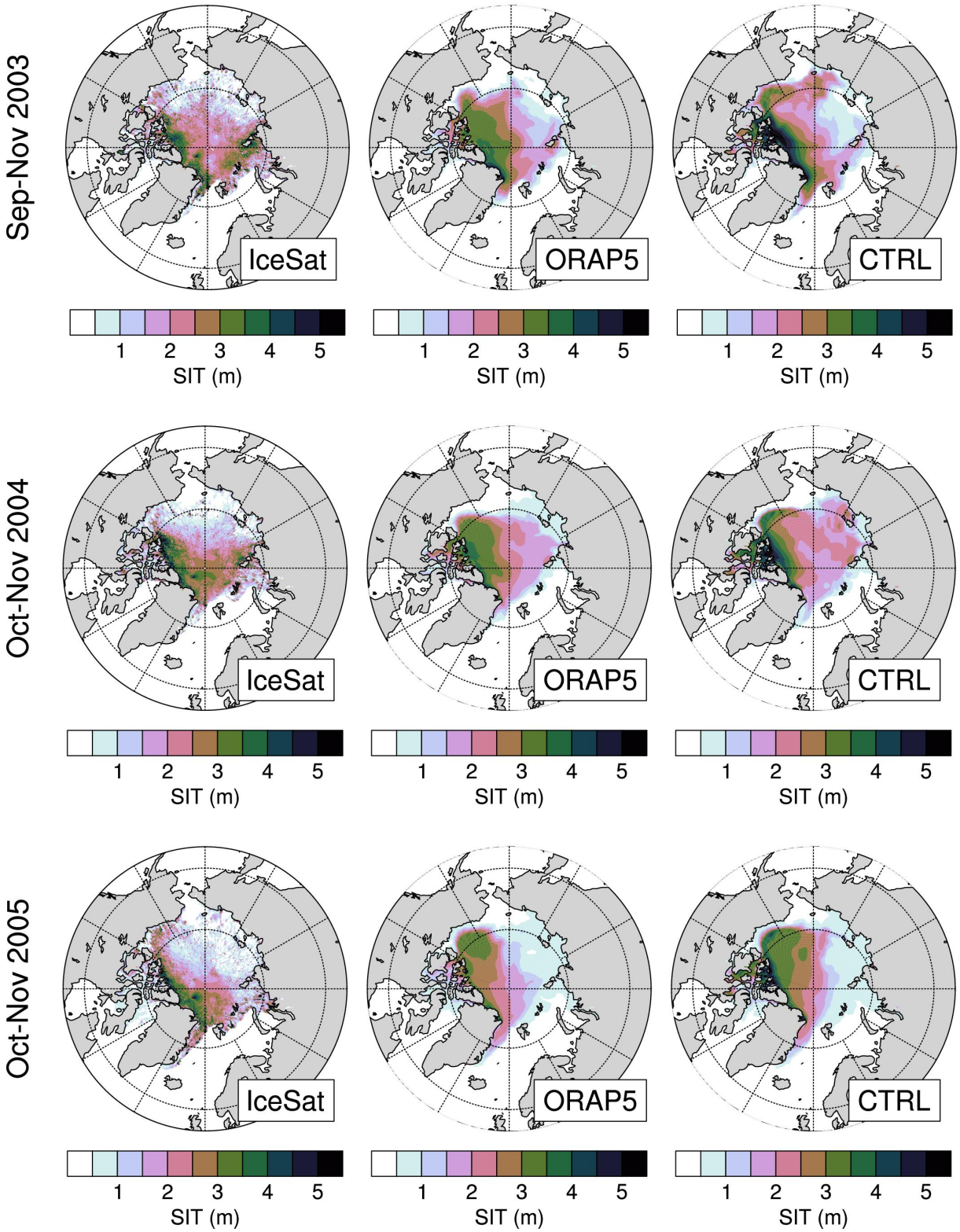

Figure 15: ICESat sea ice thickness observations (left column), ORAP5 (middle column), and CTRL (right column) for September/October/November in 2003–2005. See Table 3 for the exact dates when the observations were taken.

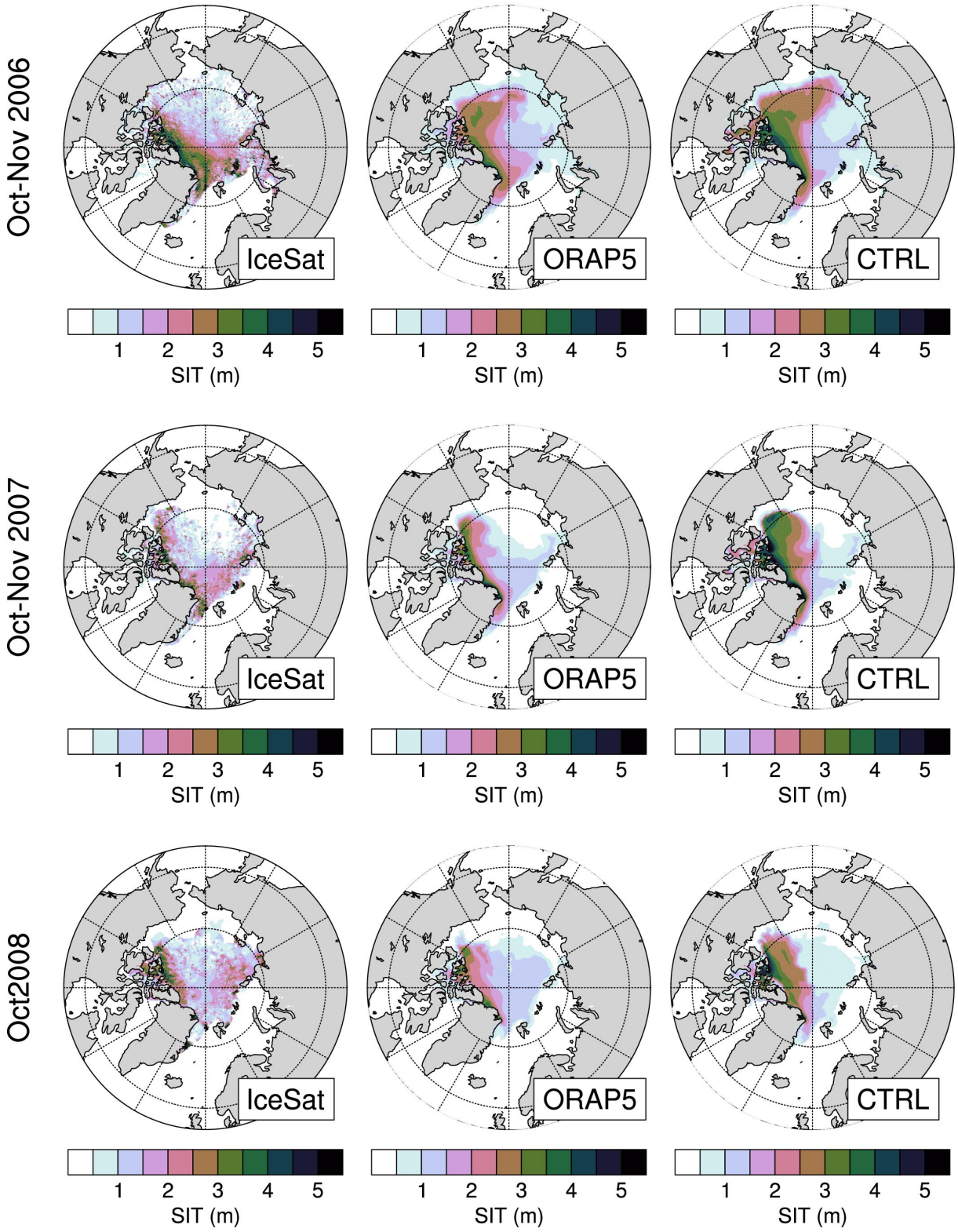

Figure 16: ICESat sea ice thickness observations (left column), ORAP5 (middle column), and CTRL (right column) for September/October/November in 2006–2008. See Table 3 for the exact dates when the observations were taken.

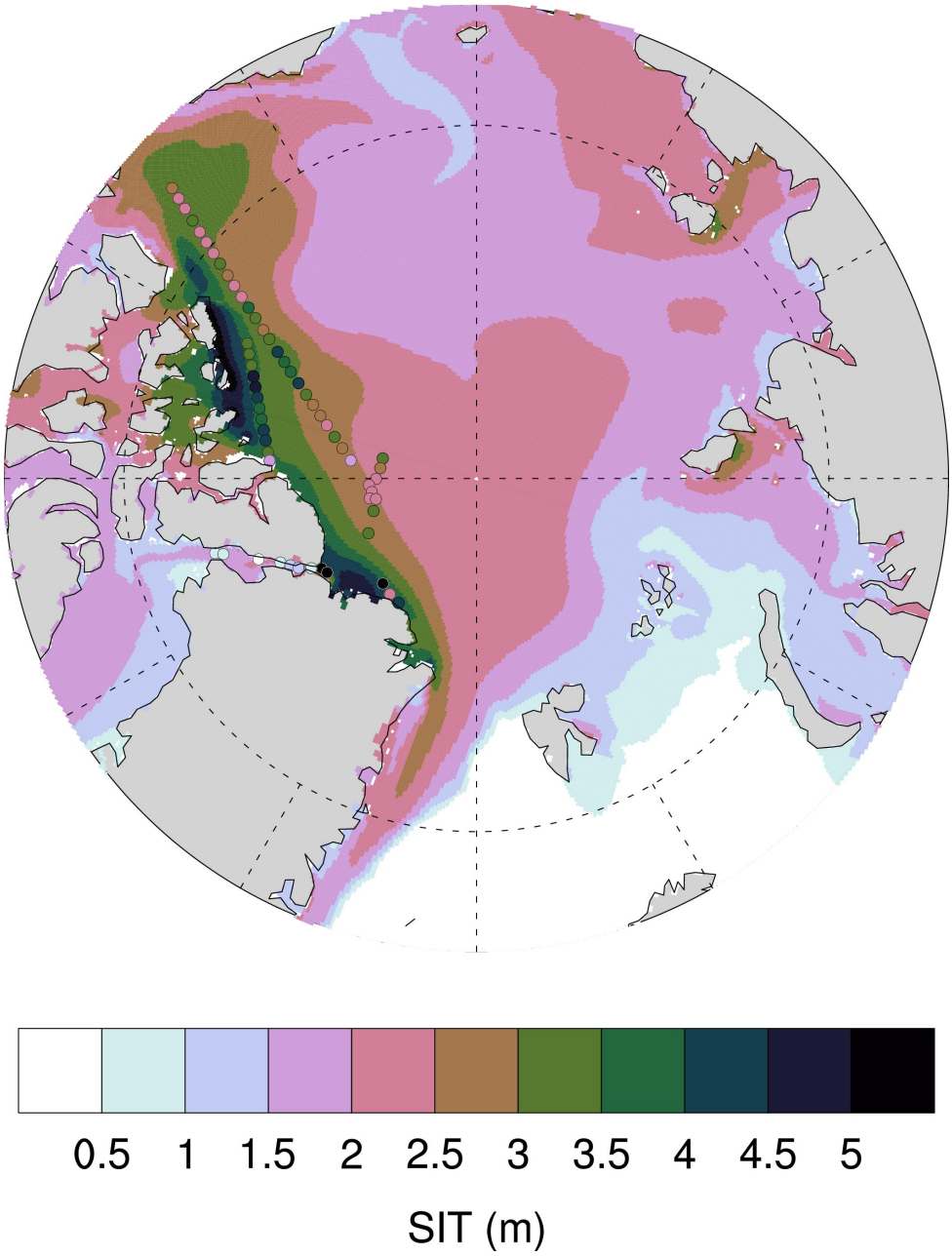

Figure 17: IceBridge ice thickness measurements from 2009/04/03 to 2009/04/25. (59 data points, coloured markers) overlayed on simulated sea ice thickness in ORAP5 for April 2009.

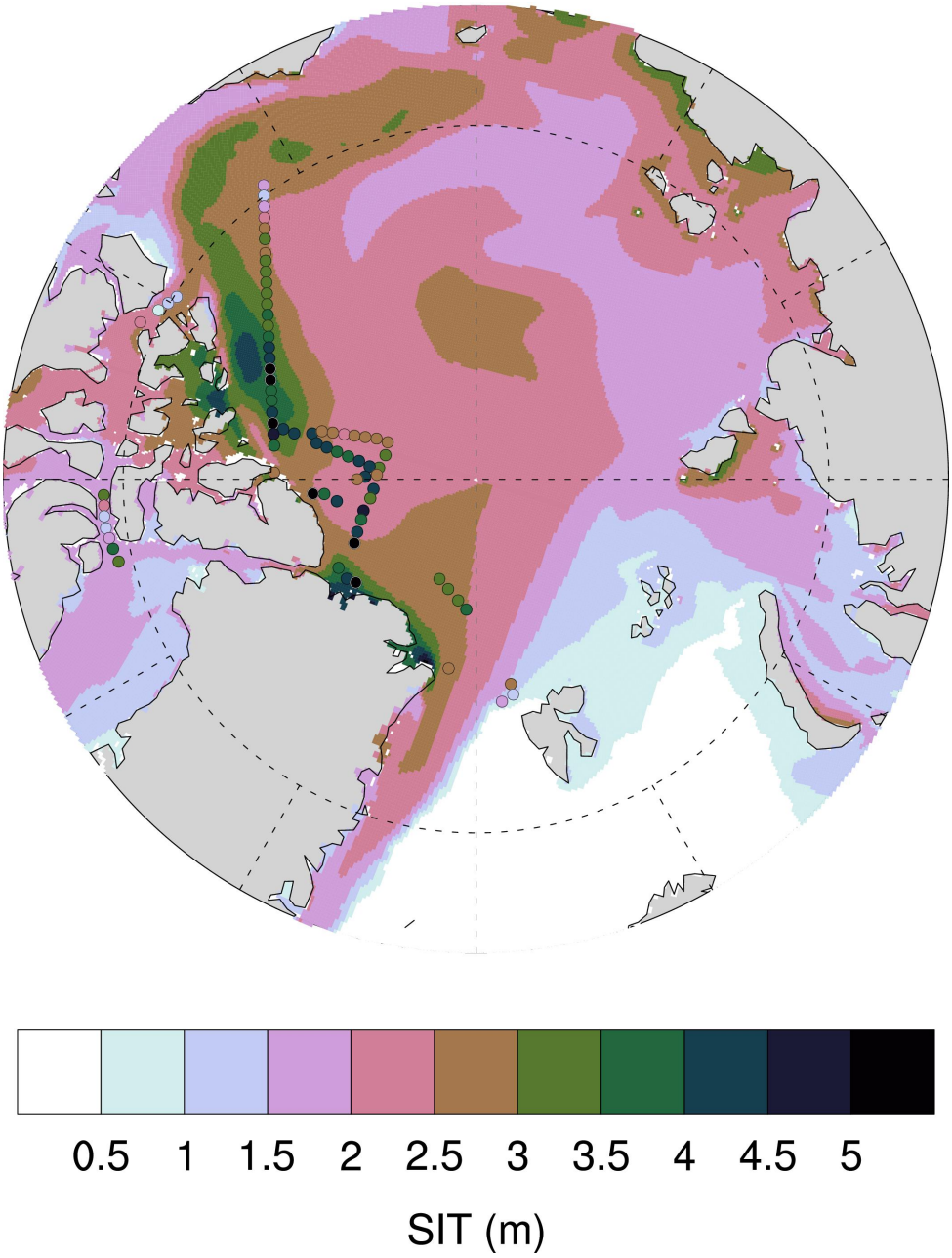

Figure 18: IceBridge ice thickness measurements from 2010/03/25 to 2010/04/05. (78 data points, coloured markers) overlayed on simulated sea ice thickness in ORAP5 for April 2010.

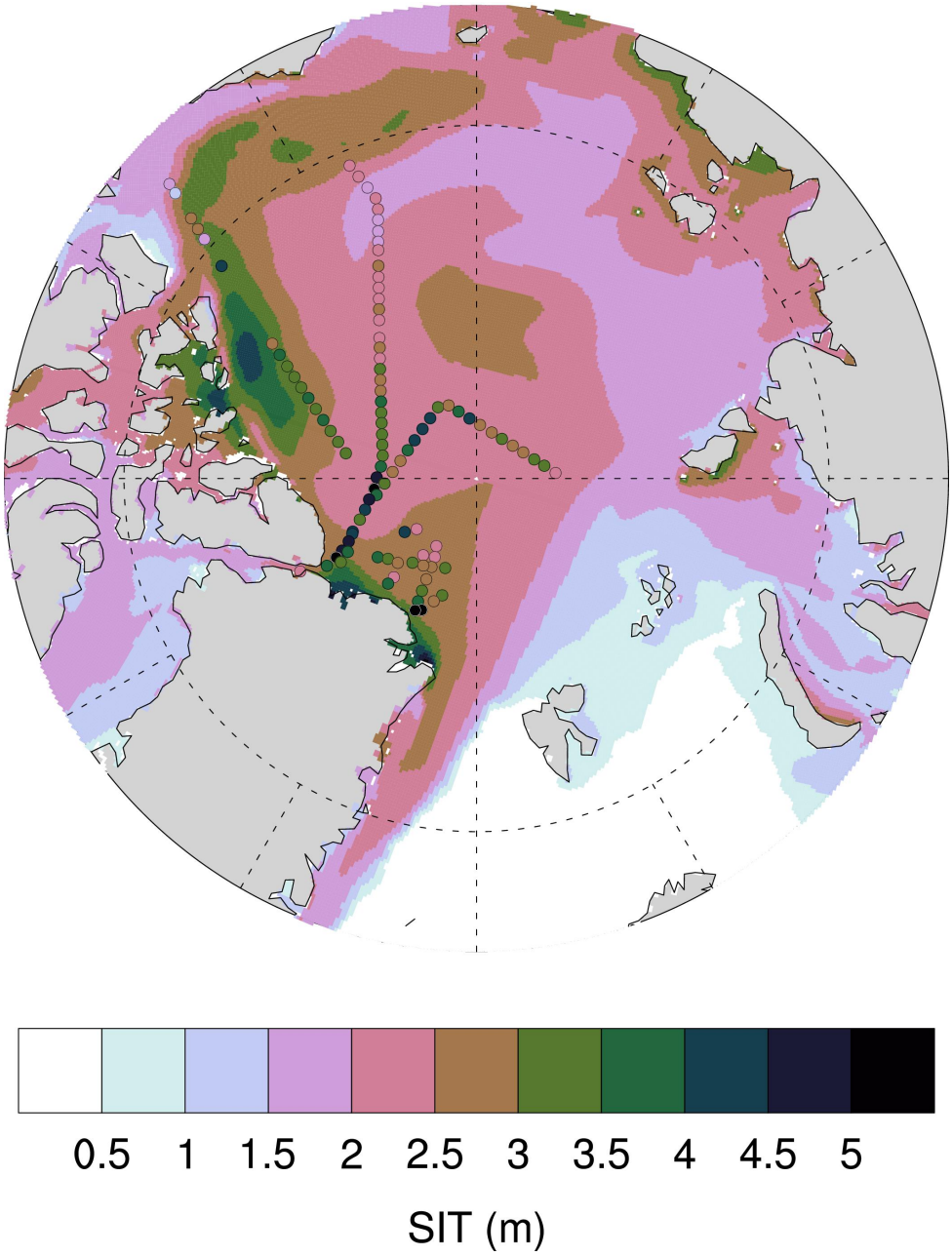

Figure 19: IceBridge ice thickness measurements from 2010/04/13 to 2010/04/21 (100 data points, coloured markers) overlayed on simulated sea ice thickness in ORAP5 for April 2010.

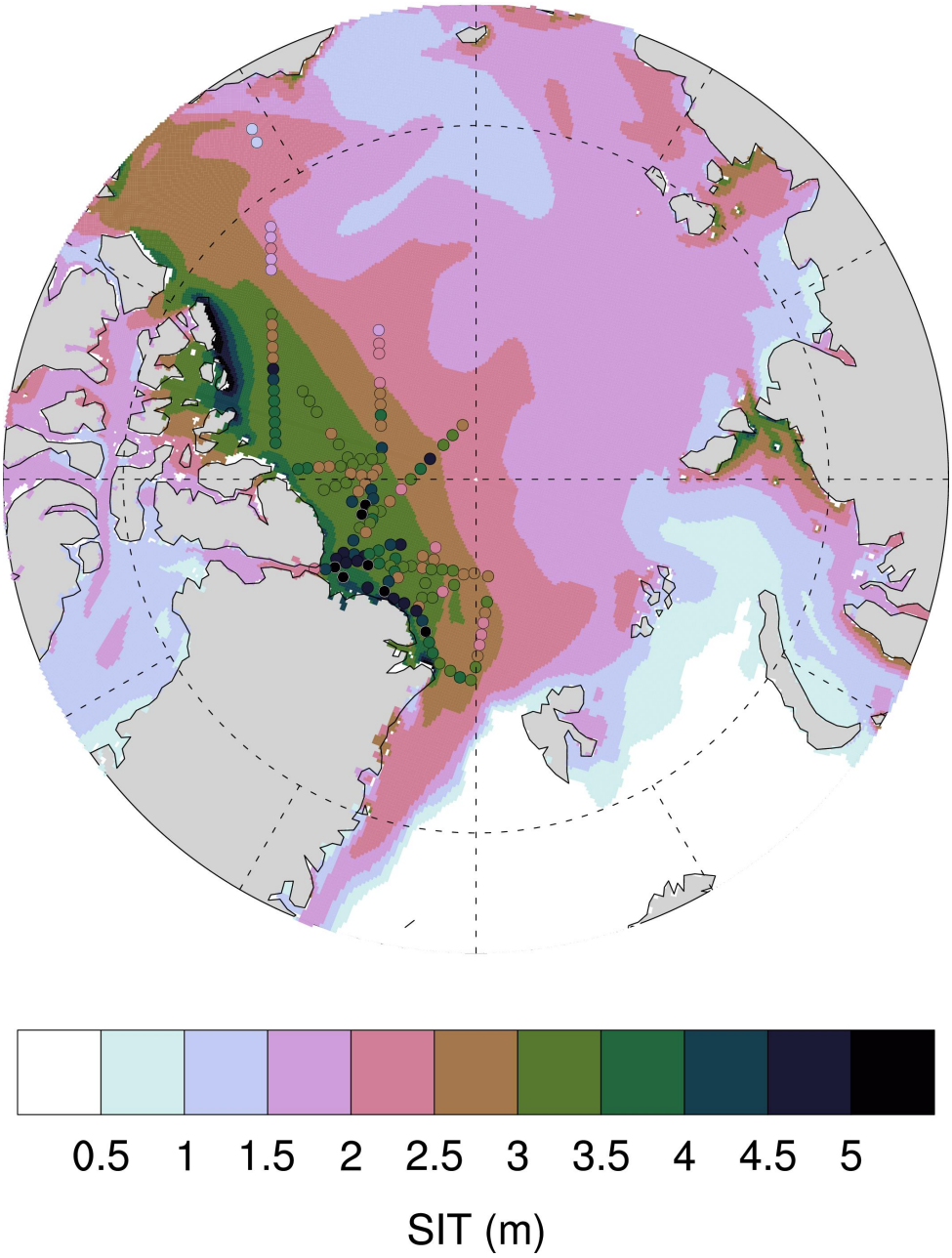

Figure 20: IceBridge ice thickness measurements from 2011/03/17 to 2011/03/29. (132 data points, coloured markers) overlayed on simulated sea ice thickness in ORAP5 for March 2011.

References

Balmaseda MA, Dee D, Vidard A, Anderson DLT. 2007. A multivariate treatment of bias for sequential data assimilation: Application to the tropical oceans. *Quarterly Journal of the Royal Meteorological Society* **133**(622): 167–179, doi:10.1002/qj.12, URL http://doi.wiley.com/10.1002/qj.12.

Balmaseda MA, Ferranti L, Molteni F, Palmer TN. 2010. Impact of 2007 and 2008 Arctic ice anomalies on the atmospheric circulation: Implications for long-range predictions. *Quarterly Journal of the Royal Meteorological Society* **136**(652): 1655–1664, doi:10.1002/qj.661, URL http://doi.wiley.com/10.1002/qj.661.

Balmaseda MA, Mogensen K, Weaver AT. 2013. Evaluation of the ECMWF ocean reanalysis system ORAS4. *Quarterly Journal of the Royal Meteorological Society* **139**(674): 1132–1161, doi:10.1002/qj.2063, URL http://doi.wiley.com/10.1002/qj.2063.

Buehner M, Caya A, Carrieres T, Pogson L. 2014. Assimilation of SSMIS and ASCAT data and the replacement of highly uncertain estimates in the Environment Canada Regional Ice Prediction System. *Quarterly Journal of the Royal Meteorological Society* : published online,doi:10.1002/qj.2408, URL http://doi.wiley.com/10.1002/qj.2408.

Cavalieri DJ, Parkinson CL, Gloersen P, Comiso JC, Zwally HJ. 1999. Deriving long-term time series of sea ice cover from satellite passive-microwave multisensor data sets. *Journal of Geophysical Research* **104**(C7): 15 803–15 814, doi:10.1029/1999JC900081, URL http://doi.wiley.com/10.1029/1999JC900081.

Chevallier M, Salas-Mélia D. 2012. The Role of Sea Ice Thickness Distribution in the Arctic Sea Ice Potential Predictability: A Diagnostic Approach with a Coupled GCM. *Journal of Climate* **25**(8): 3025–3038, doi:10.1175/JCLI-D-11-00209.1, URL http://journals.ametsoc.org/doi/abs/10.1175/JCLI-D-11-00209.1.

Comiso JC, Kwok R. 1996. Surface and radiative characteristics of the summer Arctic sea ice cover from multisensor satellite observations. *Journal of Geophysical Research* **101**(C12): 28 397–28 416, doi:10.1029/96JC02816, URL http://doi.wiley.com/10.1029/96JC02816.

Dee DP, Uppala SM, Simmons AJ, Berrisford P, Poli P, Kobayashi S, Andrae U, Balmaseda MA, Balsamo G, Bauer P, Bechtold P, Beljaars ACM, van de Berg L, Bidlot J, Bormann N, Delsol C, Dragani R, Fuentes M, Geer AJ, Haimberger L, Healy SB, Hersbach H, Hólm EV, Isaksen L, Kå llberg P, Köhler M, Matricardi M, McNally AP, Monge-Sanz BM, Morcrette JJ, Park BK, Peubey C, de Rosnay P, Tavolato C, Thépaut JN, Vitart F. 2011. The ERA-Interim reanalysis: configuration and performance of the data assimilation system. *Quarterly Journal of the Royal Meteorological Society* **137**(656): 553–597, doi:10.1002/qj.828, URL http://doi.wiley.com/10.1002/qj.828.

Donlon CJ, Martin M, Stark J, Roberts-Jones J, Fiedler E, Wimmer W. 2012. The Operational Sea Surface Temperature and Sea Ice Analysis (OSTIA) system. *Remote Sensing of Environment* **116**: 140–158, doi:10.1016/j.rse.2010.10.017, URL http://www.sciencedirect.com/science/article/pii/S0034425711002197.

Fetterer F, Knowles K, Meier W, Savoie M. 2002. Sea Ice Index 1993-2012. doi:10.7265/N5QJ7F7W, URL http://nsidc.org/data/g02135.

Fichefet T, Maqueda MAM. 1997. Sensitivity of a global sea ice model to the treatment of ice thermodynamics and dynamics. *Journal of Geophysical Research* **102**(C6): 12 609–12 646, doi: 10.1029/97JC00480, URL http://doi.wiley.com/10.1029/97JC00480.

Hibler III WD. 1979. A Dynamic Thermodynamic Sea Ice Model. *J. Phys. Oceanogr.* **9**(4): 815–846.

Ingleby B, Huddleston M. 2007. Quality control of ocean temperature and salinity profiles — Historical and real-time data. *Journal of Marine Systems* **65**(1-4): 158–175, doi:10.1016/j.jmarsys.2005.11.019, URL http://www.sciencedirect.com/science/article/pii/S0924796306002909.

Janssen P, Breivik O, Mogensen K, Vitart F, Balmaseda M, Keeley S, Leutbecher M, Magnusson L, Molteni F. 2013. Air-Sea Interaction and Surface Waves. Technical Report 712, European Centre for Medium-Range Weather Forecasts, Reading, UK.

Kaleschke L, Tian-Kunze X, MaaßN, Mäkynen M, Drusch M. 2012. Sea ice thickness retrieval from SMOS brightness temperatures during the Arctic freeze-up period. *Geophysical Research Letters* **39**(5): L05 501, doi:10.1029/2012GL050916, URL http://doi.wiley.com/10.1029/2012GL050916.

Kurtz NT, Farrell SL, Studinger M, Galin N, Harbeck JP, Lindsay R, Onana VD, Panzer B, Sonntag JG. 2013. Sea ice thickness, freeboard, and snow depth products from Operation IceBridge airborne data. *The Cryosphere* **7**(4): 1035–1056, doi:10.5194/tc-7-1035-2013, URL http://www.the-cryosphere.net/7/1035/2013/tc-7-1035-2013.html.

Kwok R, Cunningham GF. 2008. ICESat over Arctic sea ice: Estimation of snow depth and ice thickness. *Journal of Geophysical Research* **113**(C8): C08 010, doi:10.1029/2008JC004753, URL http://doi.wiley.com/10.1029/2008JC004753.

Kwok R, Cunningham GF, Wensnahan M, Rigor I, Zwally HJ, Yi D. 2009. Thinning and volume loss of the Arctic Ocean sea ice cover: 2003–2008. *J. Geophys. Res.* **114**: C07 005, doi:10.1029/2009JC005312.

Lisaeter KA, Rosanova J, Evensen G. 2003. Assimilation of ice concentration in a coupled ice–ocean model, using the Ensemble Kalman filter. *Ocean Dynamics* **53**: 368–388, doi:10.1007/s10236-003-0049-4.

Madec G. 2008. NEMO ocean engine. Technical report, Institut Pierre-Simon Laplace (IPSL), URL http://www.nemo-ocean.eu/About-NEMO/Reference-manuals.

Mellor GL, Kantha L. 1989. An ice–ocean coupled model. *J. Geophys. Res.* **94**(C8): 10 937–10 954, doi:10.1029/JC094iC08p10937.

Mogensen K, Balmaseda MA, Weaver A. 2012. The NEMOVAR ocean data assimilation system as implemented in the ECMWF ocean analysis for System 4. Technical Report 668, European Centre for Medium-Range Weather Forecasts.

Msadek R, Vecchi GA, Winton M, Gudgel RG. 2014. Importance of initial conditions in seasonal predictions of Arctic sea ice extent. *Geophysical Research Letters* **41**: 5208–5215, doi:10.1002/2014GL060799, URL http://doi.wiley.com/10.1002/2014GL060799.

Peng G, Meier WN, Scott DJ, Savoie MH. 2013. A long-term and reproducible passive microwave sea ice concentration data record for climate studies and monitoring. *Earth System Science Data* **5**(2): 311–318, doi:10.5194/essd-5-311-2013, URL http://www.earth-syst-sci-data.net/5/311/2013/essd-5-311-2013.html.

Reynolds RW, Smith TM, Liu C, Chelton DB, Casey KS, Schlax MG. 2007. Daily High-Resolution-Blended Analyses for Sea Surface Temperature. *Journal of Climate* **20**(22): 5473–5496, doi:10.1175/2007JCLI1824.1, URL http://journals.ametsoc.org/doi/abs/10.1175/2007JCLI1824.1.

Schweiger A, Lindsay R, Zhang JL, Steele M, Stern H, Kwok R. 2011. Uncertainty in modeled Arctic sea ice volume. *J. Geophys. Res.* **116**: C00D06, doi:10.1029/2011JC007084.

Semtner AJ. 1976. A Model for the Thermodynamic Growth of Sea Ice in Numerical Investigations of Climate. *J. Phys. Oceanogr.* **6**: 379–389.

Tang YM, Balmaseda MA, Mogensen KS, Keeley SPE, Janssen PEAM. 2013. Sensitivity of sea ice thickness to observational constraints on sea ice concentration. Technical Report 707, European Centre for Medium-Range Weather Forecasts, Reading.

Thorndike AS, Rothrock DA, Maykut GA, Colony R. 1975. The Thickness Distribution Of Sea Ice. *J. Geophys. Res.* **80**(33): 4501–4513.

Tian-Kunze X, Kaleschke L, MaaßN, Mäkynen M, Serra N, Drusch M, Krumpen T. 2014. SMOS-derived thin sea ice thickness: algorithm baseline, product specifications and initial verification. *The Cryosphere* **8**(3): 997–1018, doi:10.5194/tc-8-997-2014, URL http://www.the-cryosphere.net/8/997/2014/tc-8-997-2014.html.

Tietsche S, Notz D, Jungclaus JH, Marotzke J. 2013a. Assimilation of sea-ice concentration in a global climate model – physical and statistical aspects. *Ocean Science* **9**: 19–36, doi:10.5194/os-9-19-2013, URL http://www.ocean-sci.net/9/19/2013/os-9-19-2013.html.

Tietsche S, Notz D, Jungclaus JH, Marotzke J. 2013b. Predictability of large interannual Arctic sea-ice anomalies. *Climate Dynamics* **41**(9): 2511–2526, doi:10.1007/s00382-013-1698-8, URL http://link.springer.com/10.1007/s00382-013-1698-8.

Yi D, Zwally J. 2010. Arctic Sea Ice Freeboard and Thickness. URL http://nsidc.org/data/nsidc-0393.html.

Zhang J, Rothrock D. 2001. A Thickness and Enthalpy Distribution Sea-Ice Model. *Journal of Physical Oceanography* **31**(10): 2986–3001, doi:10.1175/1520-0485(2001)031⟨2986:ATAEDS⟩2.0.CO;2, URL http://journals.ametsoc.org/doi/abs/10.1175/1520-0485(2001)031<2986:ATAEDS>2.0.CO;2.

Zuo H, Balmaseda MA, Mogensen K, Haines K, Masina S, Storto A, Parent L. 2014. The ECMWF-MyOcean2 high resolution ocean reanalysis ORAP5. Technical Report 736, European Centre for Medium-Range Weather Forecasts.